Accepted Manuscript

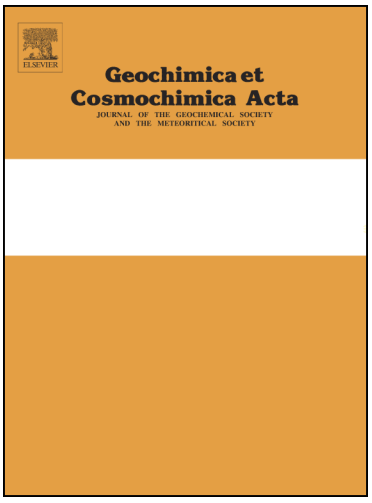

Experimental calibration of clumped isotope reodering in dolomite

Max K. Lloyd, Uri Ryb, John M. Eiler

PII: S0016-7037(18)30480-0
DOI: https://doi.org/10.1016/j.gca.2018.08.036
Reference: GCA 10909

To appear in: *Geochimica et Cosmochimica Acta*

Received Date: 7 February 2018
Revised Date: 21 August 2018
Accepted Date: 23 August 2018

Please cite this article as: Lloyd, M.K., Ryb, U., Eiler, J.M., Experimental calibration of clumped isotope reodering in dolomite, *Geochimica et Cosmochimica Acta* (2018), doi: https://doi.org/10.1016/j.gca.2018.08.036

EXPERIMENTAL CALIBRATION OF CLUMPED ISOTOPE REODERING IN DOLOMITE

Max K. Lloyd[1*], Uri Ryb[1], and John M. Eiler[1]

1. Division of Geological and Planetary Sciences, California Institute of Technology, Pasadena, CA, USA 91125

*Corresponding author: mlloyd@caltech.edu

Abstract:

Dolomite clumped isotope compositions are indispensable for determining the temperatures and fluid sources of dolomitizing environments, but can be misleading if they have modified since formation. Carbonate Δ_{47} values are susceptible to resetting by recrystallization during diagenesis, and, even in the absence of dissolution and reprecipitation reactions, alteration by solid-state reordering during prolonged residences at elevated temperatures. In order to understand the potential of dolomite Δ_{47} values to preserve the conditions of dolomitization in ancient sections, the kinetic parameters of solid-state reordering in this phase must be determined. We heated mm-sized crystals of near-stochiometric dolomite in a René-type cold seal apparatus at temperatures between 409 and 717 °C for 0.1 to 450 hours. In order to prevent the decarbonation of dolomite to calcite, periclase, and CO_2 at these conditions, the system was pressurized with CO_2 to 0.45–0.8 kbar. Over the course of 31 temperature-time points and 128 individual Δ_{47} measurements of powdered dolomite crystals from these points, we observed the evolution of dolomite Δ_{47} values from the initial (unheated) composition of the crystals (0.452 ± 0.004‰, corresponding to a formation temperature of ~145 °C) towards high-temperature equilibrium distributions. Complete re-equilbration occurred in the 563 to 717 °C experiments. As with previous heating experiments using calcite and apatite, dolomite Δ_{47} exhibited complex reordering behavior inadequately described by first-order Arrhenian-style models. Instead, we fit the data using two published models for clumped isotope reordering: the transient defect/equilibrium defect model of Henkes et al. (2014), and the exchange-diffusion model of Stolper and Eiler (2015). For both models, we found optimal reordering parameters by using global least-squares minimization algorithms and estimated uncertainties on these fits with a Monte Carlo scheme that resampled individual Δ_{47} measurements and re-fit the dataset of these new mean values. Because the exact Δ_{47}–T relationship between 250 and 800 °C is uncertain, we repeated these fitting exercises using three published high-temperature Δ_{47}–T calibrations. Regardless of calibration choice, dolomite Δ_{47} rate constants determined using both models are resolvably slower than those of calcite and apatite, and predict that high-grade dolomite crystals should preserve apparent equilibrium blocking temperatures of between ~210 and 300 °C during cooling on geologic timescales. Best agreement between model predictions and natural dolomite marbles was found when using the exchange-

diffusion model and the *ab initio* Δ_{63}–T calibration of Schauble et al. (2006), projected into the Δ_{47} reference frame by Bonifacie et al. (2017). Therefore, we recommend modeling dolomite Δ_{47} reordering using the exchange-diffusion model and this parameter set. In simple heating scenarios, the two models disagree. The transient defect/equilibrium defect model suggests that dolomite fabrics resist detectable reordering at ambient temperatures as high as 180 °C for tens of millions of years, while the exchange-diffusion model predicts incipient partial reordering perhaps as low as 150 °C. In either case, barring later recrystallization, dolomite Δ_{47} values should be faithful recorders of the conditions of dolomitization in sedimentary sections buried no hotter than ~150 °C for tens of millions of years.

1. Introduction

Dolomite is pervasive in the rock record, yet largely absent from surface sites of active carbonate precipitation. Although modern seawater is supersaturated with respect to dolomite, it appears that that sluggish crystallization kinetics inhibit dolomite precipitation at surface conditions—i.e., dolomite is out-competed by other carbonate phases unless fluid compositions are uniquely favorable to precipitation of this high-Mg carbonate (Arvidson and Mackenzie, 1999; Machel, 2004; Warren, 2000). On the other hand, models of precipitation rate suggest that even small temperature increases will preferentially raise dolomite crystallization rates with respect to calcite, which may contribute to the often-observed pseudomorphic replacement of calcite by dolomite during early diagenesis (Arvidson and Mackenzie, 1999). Temperature is by no means the only parameter regulating dolomite formation; fluid chemistry, rock porosity, water/rock ratio, and the interplay between dissolution, diffusion, and precipitation all have roles in determining when and where dolomite forms (Gregg et al., 2015; Jonas et al., 2015; Machel, 2004; Warren, 2000; Blättler et al., 2015). Nevertheless, constraining the temperatures of dolomitization is critical for evaluating competing models for this process (e.g., Murray and Swart (2017)).

Carbonate clumped isotope thermometry is a relatively new technique based on the homogeneous exchange of heavy isotopes of carbon and oxygen in aqueous carbonate groups, which are precipitated and preserved as carbonate minerals (Ghosh et al. (2006); also see reviews by Eiler (2011; 2007)). The net equation describing the distribution of these isotopes in dolomite is:

$$CaMg(^{13}C^{16}O_3)_2 + CaMg(^{12}C^{18}O^{16}O_2)_2 = CaMg(^{13}C^{18}O^{16}O_2)_2 + CaMg(^{12}C^{16}O_3)_2. \quad (1)$$

The equilibrium constant for this reaction is determined by measuring the Δ_{47} value of CO_2 produced through the digestion of carbonate in phosphoric acid by dual-inlet isotope ratio mass spectrometry. The Δ_{47} value (reported in ‰) is approximated as:

$$\Delta_{47} = R^{47}/R^{47*} - 1, \quad (2)$$

where R^{47} is the measured abundance ratio of CO_2 isotopologues of mass 47 Da (primarily $^{13}C^{18}O^{16}O$) to the unsubstituted species ($^{12}C^{16}O_2$ at 44 Da), and R^{47*} is the expected ratio for a stochastic distribution of these isotopologues (Wang et al.,

2004). Δ_{47} values of lab-grown dolomites are dependent on precipitation temperature, and thus Δ_{47} values in natural materials can be used to estimate the temperature of (re)crystallization (Bonifacie et al., 2017; Ghosh et al., 2006).

Using this technique, dolomitization in extant carbonate platforms has been observed at a range of subsurface depths and temperatures, from soon after deposition to later recrystallization in Mg-rich brines at 15–70 °C (Murray and Swart, 2017; Winkelstern and Lohmann, 2016). Estimates of $\delta^{18}O$ values of the fluids in equilibrium with these phases, a useful consequence of Δ_{47}-derived temperature determinations, can further constrain the conditions of dolomite formation (Murray and Swart, 2017). This approach may be especially useful for interrogating the conditions of dolomite formation in ancient sections, where far less is known about the chemistry of seawater and seawater-derived brines (Bergmann, 2013; Ferry et al., 2011). However, most ancient carbonate platforms have been subjected to protracted burial diagenesis and low-grade metamorphism, which could alter Δ_{47} compositions. Interpretation of dolomite Δ_{47}–derived temperatures and fluid $\delta^{18}O$ contents in these sections requires knowledge of the conditions under which they can be modified.

1.1 Solid-state reordering in carbonate minerals

Fine-grained carbonate fabrics are susceptible to recrystallization during diagenesis (Shenton et al., 2015; Winkelstern and Lohmann, 2016). During deep burial and low-grade metamorphism, cryptic dissolution and reprecipitation can even reset Δ_{47} values while preserving early diagenetic textures (Cummins et al., 2015; Lloyd et al., 2017; Shenton et al., 2015). Even in the absence of recrystallization, primary carbonate clumped isotope temperatures can be obscured by solid-state reordering, defined as the diffusion and exchange of heavy isotopes of carbon and oxygen in intact crystals in order to re-equilibrate with new ambient temperatures (Dennis and Schrag, 2010; Passey and Henkes, 2012). The kinetics of carbonate clumped isotope reordering have been determined in apatite and a variety of calcites by observing the time-dependent changes in Δ_{47} values as low-temperature configurations approach high-temperature equilibrium while held in furnaces at fixed temperatures between 385 and 692 °C (Henkes et al., 2014; Passey and Henkes, 2012; Stolper and Eiler, 2015). Extrapolation of the Arrhenian parameters derived from these experiments suggests that calcite crystals are susceptible to detectable amounts of reordering, and therefore the formation temperatures within are compromised, when heated to ambient temperatures as low as 100 °C for tens of millions of years (Stolper and Eiler, 2015).

Apparent equilibrium blocking temperatures in slowly-cooled dolomite marbles—i.e., the diffusion-limited concentration of ^{13}C–^{18}O bonds preserved when a high-temperature phase internally re-equilibrates with progressively lower temperatures during cooling—are ~100 °C higher than those in coexisting calcite marbles (250–300 °C vs. 150–200 °C), which suggests that the rates of solid-state clumped isotope reordering in dolomite are slower than in calcite (Bonifacie et al., 2011; Eiler, 2011; Ferry et al., 2011; Lloyd et al., 2017; Ryb et al., 2017). If so,

dolomite Δ_{47} records should be more resistant to alteration during burial and heating, and could be accurate archives of the conditions of dolomitization in ancient sections. Here, we report a series of heating experiments using fragments of a dolomite megacryst in order to determine the rate constants for dolomite Δ_{47} solid-state reordering. We use these parameters to predict to the susceptibility of the dolomite Δ_{47} thermometer to alteration during deep burial and metamorphism.

1.2 Contrasting models for solid state reordering

An additional motivation for this study is to address outstanding questions regarding the mechanism for such re-equilibration and the primary controls on its rate. Time–Δ_{47} trends in all published lab-based heating experiments are inadequately described by first-order rate equations. Instead, models to fit the calcite and apatite Δ_{47} reordering data require a transient mechanism for initial, rapid re-equilibration superimposed upon a persistent, 'background' reordering rate (Henkes et al., 2014; Passey and Henkes, 2012; Stolper and Eiler, 2015). Although calibrated to results that are statistically indistinguishable, the two existing models have distinct physical groundings that lead to contrasting interpretations of the behavior of the clumped isotope thermometer in natural settings.

Based on the widely-held view that atomic diffusion in minerals is facilitated by structural defects (Zhang, 2010), Henkes et al. (2014) attribute initial, non-first order reordering to a high concentration of crystallographic defects in low-temperature crystals. In their model, many of these defects are annealed during prolonged heating, which reduces the mobility of carbonate components and progressively slows the reordering rate. The time-invariant reordering rate observed during later stages of these heating experiments thus reflects the concentration of un-annealable defects (e.g., cation substitutions, vacancies). This interpretation suggests that every carbonate grain should have a unique susceptibility to solid-state reordering that is emblematic of its specific defect concentration, and that for high-temperature materials, only equilibrium defects need be considered. Nonetheless, all calcite minerals considered so far have similar equilibrium reordering rates that appear to be independent of Mn concentration, crystallization environment, and other external constraints on possible contributors to the 'equilibrium' defect concentration.

The model proposed by Stolper and Eiler (2015) attributes non-first order Δ_{47} reordering behavior to physical limits on reordering rate imposed by the geometry of the calcite crystal lattice. Specifically, they hypothesize that changes in clumped isotope composition occur through exchange of heavy C and O isotopes only among neighboring carbonate groups. Thus although initial, rapid partial re-equilibration readily occurs in unit cells where both ^{13}C and ^{18}O are present in neighboring carbonate groups (defined by the authors as 'pairs'), complete re-equilibriation is rate-limited by the diffusion of ^{13}C or ^{18}O-bearing groups (defined as 'singleton')

through the crystal lattice. Unlike the Henkes et al. (2014) model, this construction implies that the capacity of carbonate minerals to partially re-equilibrate Δ_{47} by the non-first order mechanism is an intrinsic feature of the system. Thus, rapid initial changes in Δ_{47} in response to changing conditions should occur during both the heating of cold carbonates and the cooling of hot ones, provided some excess of pairs persists.

Estimates of calcite Δ_{47} compositions from both models are consistent with compositions of reordered natural materials, but those of apatite Δ_{47} compositions are not (Stolper and Eiler, 2015). In carbonatites, apatite apparent equilibrium blocking temperatures are 40–60 °C colder than those of coexisting calcite (Stolper and Eiler, 2015). Parallel heating experiments, however, predict that apatite Δ_{47} values should preserve apparent temperatures 30–50 °C above calcite Δ_{47} values during the cooling of high-temperature igneous or metamorphic rocks (Stolper and Eiler, 2015). The cause of the disagreement between measured and modeled apatite Δ_{47} values is not established, but may be due to accelerated reordering through the accumulation of radiation damage (Stolper and Eiler, 2015), or could reflect an incomplete understanding of the spatial distribution or bonding environment of carbonate groups in this mineral (Kolodny and Kaplan, 1970). On the other hand, the apparent agreement between natural and experimental reordered calcite Δ_{47} rates could be fortuitous, and the mechanisms for Δ_{47} reordering could be broadly misunderstood. Testing the agreement between modeled and observed apparent equilibrium Δ_{47} values in a new mineral phase may indicate which of the above statements is more likely, and could resolve outstanding questions regarding the controls on clumped isotope reordering rate.

2. Materials and methods

In order to directly compare dolomite and calcite Δ_{47} reordering rates, we replicated the experimental design and measurement conditions of Stolper and Eiler (2015) as closely as possible. The following methods description emphasizes conditions unique to these dolomite experiments.

2.1 Sample selection

Because Δ_{47} signals of fine-grained carbonate fabrics are vulnerable to overprinting during dissolution-reprecipitation reactions at grain boundaries, large, homogeneous crystals are preferable for high-temperature reordering experiments. However, the precipitation of coarse dolomite crystals is kinetically limited at near-surface temperatures. Large (>10 cm), high-temperature crystals, on the other hand, are resolved in Δ_{47} value from the equilibrium infinite-temperature limit by only a small multiple of the typical uncertainty on replicate Δ_{47} measurements and are thus inadequate for measuring rate constants with useful precision. As a compromise between these competing needs, we used an aggregate of cm-sized, translucent, rhombohedral dolomite crystals that formed in an open fissure from hydrothermal fluids at somewhat elevated temperatures in Eugui, Spain. The type locality for optical-quality dolomite (Lugli et al., 2000), Eugui dolomite is compositionally

homogeneous, near-perfectly stoichiometric, well-ordered, and largely free of structural defects (Barber et al., 1981; Navrotsky and Capobianco, 1987; Reeder and Nakajima, 1982; Reeder and Wenk, 1983). It has been the starting material for a large number of investigations of dolomite crystallinity, thermal stability, deformation and dissolution rates (Barber et al., 1981; Chai and Navrotsky, 1996; Martinez et al., 1996; Reeder and Markgraf, 1986; Urosevic et al., 2012), and a reference standard against which the physical and chemical properties of sedimentary and saddle dolomites are compared (Barber et al., 1985; Jones et al., 2001). Given the paucity of ordered, stochiometric, megacrystic dolomite in nature, and the utility of direct comparison of Δ_{47} reordering rates to other properties of this well-characterized sample, we suggest that the Eugui dolomite is an appropriate material for these experiments, provided its initial Δ_{47} composition is sufficiently uniform and resolved from the equilibrium high-temperature limit.

Our sample of Eugui dolomite was acquired from Susan M. Ulrich Fine Minerals. The sample is a ~900 g, ~8 x 8 x 5 cm aggregate of transluscent, rhombohedral crystals 1–3 cm across, protruding from a base of massive, white crystalline dolomite (Supplementary Fig. S1). The mineralogy and crystallinity of this material were confirmed by powder X-ray diffractometry (XRD). Briefly, a single crystal from the aggregate was broken off, powdered, and analyzed using a Bruker Phaser D2 XRD with a 20 KeV beam, 20–60 2-theta scan range, 0.05 step size, and 0.5 s integration time. The locations and widths of scan peaks are consistent with well-ordered dolomite.

2.2 Elemental and isotopic composition and homogeneity

The elemental abundances of one colorless, mm-sized fragment the primary aggregate and one fragment from the white crystalline base were measured on a JEOL JXA-8200 electron probe micro-analyzer. Using a 15 KeV beam, with a 20 nA beam current, and a 10 μm spot size, the concentrations of the oxides of CaO, MgO, FeO, and MnO were determined for ten spots on each fragment, and standardized against analyses of dolomite, siderite, and rhodochrosite from the same analytical session. Averages and standard deviations of these measurements for each crystal are reported in Table S1. Using the measured oxide abundances and an assumed CO_2 content, we derive a formula for the colorless crystal that is nearly stoichiometric dolomite: $Ca_{0.500}Mg_{0.493}Fe_{0.006}Mn_{0.001}(CO_3)_{1.0}$. The white dolomite material from the base of the sample has a comparable stoichiometry, with a lower Fe content (0.294 ± 0.056 mol. %) and a similar Mn content (0.126 ± 0.018 mol. %).

In order to determine the isotopic composition of the acquired sample and test its homogeneity, we cleaved translucent, faceted, crystal fragments from three distal locations on the crystal aggregate. We additionally extracted material from a large, white crystal at the base of the aggregate and from two locations on the white-gray, massive, polycrystalline dolomite matrix below it in order to compare the colorless, faceted crystals (which are the experimental material of our study) to their host carbonate (Supplementary Fig. S1). Care was taken to avoid, or physically abrade, a soft, red-tan powder found at base of the crystal aggregate. Fragments from each of

these six sites were powdered, dry, in an agate mortar and pestle to < 106 μm, and analyzed for $\delta^{13}C$, $\delta^{18}O$, and Δ_{47} content using standard procedures for automated digestion, purification, and measurement by dual-inlet isotope ratio mass spectrometry, outlined below (Section 2.3) and described in detail elsewhere (e.g., Passey et al. 2010). Mean carbonate Δ_{47} values from each site agree within 2σ standard errors of replicate measurements, suggesting that the entire sample, including the massive crystalline base, formed at approximately uniform conditions, with a Δ_{47} value of 0.452 ± 0.003 ‰ (1σ std. error, n = 31, reported in the absolute reference frame (ARF); Dennis et al., 2011). The bulk ^{13}C and ^{18}O contents vary among sample sites: $\delta^{13}C$ values are confined to a relatively narrow range of +2.19 to + 2.78 ‰ (vs. VPDB); $\delta^{18}O$ values of the translucent crystal aggregate are similarly uniform ($\delta^{18}O_{VPDB}$ of –13.66 to –13.34 ‰), but significantly higher than those of the massive dolomite base (as low as –16.47 ± 0.95 ‰). Heterogeneity in bulk isotope composition is potentially problematic because materials with distinct carbon-13 and oxygen-18 contents, but similar Δ_{47} values, do not mix linearly (Eiler and Schauble, 2004). Such non-linear mixing effects, however, are insignificant for the compositional variations reported here: physical mixtures of dolomite domains with identical Δ_{47} compositions, nearly identical $\delta^{13}C$ values, but ~3 ‰ differences in $\delta^{18}O$ will generate apparent enrichments in Δ_{47} of at most 0.0003 ‰; such discrepancies are a small percentage of typical analytical uncertainty and thus functionally undetectable. Even so, due to the differences in mineral habit, coloration, and Fe content between the colorless crystal aggregate and the fine white dolomite at its base, and the uncertainty regarding how such differences might affect reordering rate, we used only fragments of the colorless aggregate for our heating experiments. This habit appears to be nearly homogeneous with respect to all three measured isotopic parameters, and thus may be an appropriate material for the present study.

2.3 Heating experiments

Because dolomite is thermodynamically unstable at atmospheric pressure at the temperatures of the reordering experiments, all experiments were performed at elevated pressures in a rapid-quench, metal René-type cold seal apparatus (Blank et al., 1993), the exact same apparatus used for the calcite heating experiments of Stolper and Eiler (2015). For each run, two to eight mm-sized fragments from the colorless aggregate of dolomite crystals (total mass: 47–91 mg) were placed in an unsealed platinum capsule, affixed to the end to an iridium rod using platinum wire, and sealed into the water-cooled chamber of the cold seal apparatus. The system was pressurized, placed in a resistance furnace set to the target temperature for each run, and allowed to thermally equilibrate for at least two hours. Each reordering experiment began by raising the iridium rod and platinum capsule into the heated end of the cold-seal tube using a magnetic collar. Each experiment was terminated by removing the collar, which dropped the Pt capsule into the water-cooled jacket and quenched the samples to ~20 °C in 1–2 seconds. Following each experiment, the system was depressurized, the crystals were retrieved, and the

reusable Pt capsule was sonicated in 5 N HCl for 10 minutes to remove any residual carbonate.

In an initial run pressurized with Ar to 67.6 MPa at 717 °C for 5 minutes, dolomite decarbonation occurred: at the end of the experiment, crystals were coated in a fine, white powder, and had undergone a mass loss of 3.8 %. Previous experiments have demonstrated that at these conditions, dolomite dissociates to periclase and calcite by the (simplified) reaction (Goldsmith and Heard, 1961; Graf and Goldsmith, 1955):

$$CaMg(CO_3)_2 \rightarrow CaCO_3 + MgO + CO_2. \quad (3)$$

Note that the empirical reaction is more complicated because the impure product calcite lies on a solid solution with $MgCO_3$, and its exact stoichiometry is dependent on temperature and the partial pressure of CO_2 (pCO_2) (Graf and Goldsmith, 1955). At 717 °C, dolomite is stable at pCO_2 values above ~15 MPa but below ~3 GPa, where it dissociates into aragonite and magnesite (Goldsmith and Heard, 1961; Graf and Goldsmith, 1955; Shirasaka et al., 2002). So, in subsequent runs, we pressurized the cold seal apparatus with 43.5–78.4 MPa of CO_2 instead of Ar. We monitored for decarbonation in these experiments with high-magnification imagery and mass measurements before and after each run. When using CO_2 as headspace gas, no visible decarbonation occurred and mass loss was limited to at most 1.6% but typically ~0.6%, which we attribute to incomplete recovery of small crystal fragments.

During the first heating experiment pressurized with CO_2 (at 717 °C, 64.2 MPa, 5 minutes), the Pt capsule, wire, Ir rod, and dolomite crystals were coated with a lustrous grey-black patina, presumably a graphitic residue resulting from the oxidation of the inner metal surfaces of the cold seal pipe. A reaction between the cold seal surfaces and CO_2 is further implicated because the patina was restricted to the hot end of the Ir rod, and was thicker on the outer surfaces of the Pt capsule than the inner surfaces. During subsequent runs progressively less deposition occurred, and after ten heating experiments graphitic coatings were no longer observed. To preclude contamination of carbonate samples by a deposited carbon source, we removed the graphitic coating by sonicating crystals in acetone for 15 minutes, then evaporating the acetone overnight in a fume hood. Control tests using unheated crystals demonstrated no change in mass or isotopic composition as a result of this cleaning procedure.

In total, we conducted thirty-one heating experiments with CO_2 pressures of 43.5–78.4 MPa at temperatures between 409 and 717 °C for times between 0.125 and 455 hours. Temperature accuracy was tested by measuring the temperature inside the heated end of the cold seal pipe while the apparatus was equilibrated in the resistance furnace using a calibrated type-K thermocouple inserted through the open, cold, bottom of the pipe. A steep thermal gradient was observed between the hot, top of the pipe and the water-cooled midpoint 20 cm below. We calibrated this gradient by measuring the temperature in the pipe in 1 cm increments over a 4 cm

section enveloping the location where the samples reside in the pipe at the furnace setpoints of all experiments. The average temperature over the closest (to the sample site) 2 cm section is slightly higher than but well defined by the furnace setpoint: $T_{measured} = 1.0275*T_{furnace} - 2.3929$ ($R^2 = 0.9998$). We use this calibration to estimate the temperature in the Pt capsule during each run, but note that these measurements do not exactly replicate conditions in the cold seal apparatus during heating experiments because the apparatus does not permit measurement of temperatures inside the tube when it is sealed and pressurized.

A potential concern of heating dolomite in the presence of high pCO_2 is the exchange of carbonate ions in the crystals with headspace gas. To test for this, we recovered and measured the bulk isotopic composition of tank CO_2 used in run #11 (at 511 °C, 64.6 MPa, 12.8 hours): $\delta^{13}C_{VPDB} = -41.2$ ‰, $\delta^{18}O_{VPDB} = -32.3$ ‰. Dolomite in equilibrium with this CO_2 at this temperature would have $\delta^{13}C_{VPDB}$ and $\delta^{18}O_{VSMOW}$ compositions of –44.1 and –37.1 ‰, respectively (O'Neil and Epstein, 1966; Schauble et al., 2006). Since these values are ~47 ‰ (for $\delta^{13}C$) and 23 ‰ (for $\delta^{18}O$) lower than the mean composition of the unheated dolomite crystal, we would expect even partial gas-mineral isotope exchange to dramatically shift the compositions of heated samples to lower values, and for the size of such shifts to increase with time at a given temperature. The lack of variations in $\delta^{13}C$ or $\delta^{18}O$ greater than 1 ‰ and further lack of correlations with time among all heating experiments indicate that exchange with headspace gas does not significantly contribute to the single (or presumably, clumped) isotope compositions in these runs.

2.3 Analytical methods

Cleaned, heated dolomite crystals, and their unheated counterparts, were analyzed by standard carbonate clumped isotope techniques (e.g., Passey et al. 2010). Briefly, crystals were ground, dry, with an agate mortar and pestle until entire samples passed through a 106 μm sieve. Powders were loaded into silver capsules, and digested for 20 minutes in a common acid bath of 104 % phosphoric acid held at 90 °C. We note that this powdering is necessary in order to completely react dolomite in the allotted time. Evolved CO_2 was continually separated from H_2O on a dry ice + ethanol trap held at –67 °C and frozen in liquid N_2 at –196 °C. Organic contaminants were removed by passing CO_2 through a Porapaq Q 50/80 packed mesh column held at –20 °C in a He stream at a flow rate of 15 cm^3/min. Cleaned CO_2 was analyzed at masses 44–49 on a Thermo MAT 253 dual-inlet isotope ratio mass spectrometer at Caltech against a calibrated reference CO_2 tank acquired from Oztech®.

Voltages on masses 44–48 were extracted from binary measurement files and reduced to $\delta^{13}C_{VPDB}$, $\delta^{18}O_{VPDB}$, and raw Δ_{47} values using a Python script that is publicly available and regularly updated (www.github.com/maxmansaxman/clumpy). $\delta^{13}C$ and $\delta^{18}O$ values (and by extension, raw Δ_{47} values) were calculated using the Brand et al. (2010) reference parameters recommended by Daëron et al. (2016) and Schauer et al. (2016) and the

Taylor polynomial method described by Daëron et al. (2016). In each 1–3 week session, raw Δ_{47} values were corrected for nonlinearities and source scrambling, and projected into the absolute reference frame (ARF) using contemporaneous 1000 °C-equilibrated CO_2 gases that were measured daily and 25 °C-equilibrated gases that were measured 4x per week (Dennis et al., 2011). Two intralaboratory carbonate standards were measured daily to independently monitor the stability and accuracy of the reference frame.

Dolomite $\delta^{18}O_{VPDB}$ values were calculated from $\delta^{18}O_{VPDB}$ values of measured CO_2 using the predicted dolomite–CO_2 ^{18}O phosphoric acid fractionation interpolated to 90 °C from a 2nd-order polynomial fit to the 25 °C, 50 °C, and 100 °C fractionations from Rosenbaum and Sheppard (1986). Δ_{47} values of these 90 °C reactions were corrected to the canonical 25 °C scale by adding a 90 °C phosphoric acid fractionation factor of 0.092 ‰ (Henkes et al., 2013). This value is significantly lower than the dolomite Δ_{47} acid fractionation suggested by Murray et al. (2016); however, as demonstrated by Bonifacie et al. (2017), discussed in Lloyd et al. (2017), and further supported by the high-temperature equilibration experiments of the present study (see below), it appears that dolomite and calcite have indistinguishable Δ_{47} acid fractionations on the carbonate clumped isotope systems at Caltech.

As will be shown below, kinetic parameters derived from heating experiments are sensitive to the Δ_{47}–temperature calibration used. Thus, we report Δ_{47}-derived temperatures, calculate equilibrium Δ_{47} values for heating experiments, and forward-model cooling dolomite marbles using three Δ_{47}–T calibrations suitable for high temperature studies: briefly, a 2nd-order polynomial fit to natural and experimental carbonate data from Bonifacie et al. (2017) (hereafter, the 'Bonifacie calibration'), a 2nd-order polynomial fit to calcite and dolomite Δ_{47} data generated solely at Caltech from Lloyd et al. (2017) ('Lloyd calibration'), and an *ab initio* model for equilibrium ^{13}C–^{18}O clumping in carbonates calculated in Schauble et al. (2016) and transferred into the CO_2 reference frame in Bonifacie et al. (2017) ('Schauble + Bonifacie calibration').

First, we fit all data using eqn. 2 from Bonifacie et al. (2017), which is a 2nd-order polynomial fit to natural and experimental dolomites and calcites equilibrated at 25–1600 °C, most of which were measured at Caltech on the same instrument of the present study (Bonifacie calibration). Although this equation is not recommended for low-temperature materials, calculating Δ_{47} reordering rate constants requires a continuous Δ_{47}–T function spanning the entire range over which Δ_{47} values are measured. We note that although we report Δ_{47} values adjusted to the legacy 25 °C acid scale, the employed Δ_{47}–T equation is explicitly calibrated for carbonates reacted at 90 °C, as these are here.

Although eqn. 2 from Bonifacie et al. (2017) fits Δ_{47} data measured in multiple laboratories over a wide range of temperatures, there is significant disagreement between experimental data and the polynomial fit at the temperatures most critical for our dolomite reordering: because the regression is strongly influenced by Δ_{47}

values of older calcite re-equilibration experiments of Passey and Henkes (2012), it misses the study's own high temperature dolomite precipitation experiments by as much as 0.02‰ (Fig. 4 in Bonifacie et al., 2017). So, we also fit our data using the 2nd-order polynomial equation of Lloyd et al. (2017) (Lloyd calibration). This equation is calibrated to a subset of the data used in the Bonifacie et al. (2017) 2nd-order fit, which were measured exclusively at Caltech on the same instruments as the present study. Thus, it avoids systematic errors that may be introduced by incorporating data from multiple labs with different experimental setups and data processing schemes. On the other hand, because it employs data produced in a single facility, the Lloyd et al. (2017) calibration may not be universally useful for other users.

As discussed in Bonifacie et al. (2017), the *ab initio* equilibrium dolomite and calcite Δ_{63}–T relationships predicted by Schauble et al. (2006) agree remarkably well with the Δ_{47} values of all reported dolomite precipitation experiments when a carbonate–CO_2 90 °C acid fractionation factor of 0.176‰ is added. So, we also fit our reordering data with Δ_{47} values calculated using this equation, in order to test whether it more accurately represents the Δ_{47}–T relationship in the realm of 300–800 °C (Schauble + Bonifacie calibration). Specifically, all equilibrium Δ_{47} values, reaction progress variables, and predicted reordering capacities we re-calculated using the equation:

$$\Delta_{47,ARF90} = \frac{-3.4075e^9}{T^4} + \frac{2.3655e^7}{T^3} - \frac{2.6317e^3}{T^2} - \frac{5.8537}{T} + 0.176\,, \qquad (4)$$

where T is in kelvin, and $\Delta_{47,ARF90}$ is in ‰ (Schauble et al., 2006; Bonifacie et al., 2017). Because the inverse equation (T in terms of Δ_{47}) has no analytical solution, it is estimated using 5 iterations of the Newton-Raphson method. Note that although this equation is specifically calibrated for calcite, predicted calcite and dolomite Δ_{63}–T relationships agree within 0.004‰ above 30 °C, and within 0.001‰ above 150 °C. So, given typical analytical uncertainties, the choice of calcite or dolomite Δ_{47}–T *ab initio* calibration makes no difference at the temperatures of interest here. Conversely, because the Schauble + Bonifacie calibration predictions are consistently lower in Δ_{47} than the Bonifacie calibration by 0.010–0.015 ‰ between 300 and 500 °C, but in adequate three-way agreement (all within 0.005 ‰) between 40 and 240 °C, the choice of Δ_{47}–T calibration matters greatly for fitting our dolomite reordering data, but not significantly for forward-modeling Δ_{47} reordering in sedimentary basins.

In Section 5, we find that fits generated using the Schauble + Bonifacie Δ_{47}–T calibration are in better agreement with natural observations of reordered dolomite than the other two. So, in the following description of the results of fitting routines, Eqn. 4 is implicitly used for all calculations unless otherwise noted. Nonetheless, fitting parameters using all three calibrations are reported in the data tables below.

3. Results of dolomite reordering experiments

Thirty-one heating experiments were performed on fragments of translucent Eugui dolomite crystals at temperatures between 409 °C and 717 °C, under CO_2 pressures of 43.5 to 78.4 MPa, for times between 0.125 and 455 hours. Powders from these experiments and the unheated starting material were measured during nine analytical sessions over the course of two years. Thirty-five measurements of unheated powders from these nine sessions tightly constrain the initial Δ_{47} composition to 0.452 ± 0.002 ‰, corresponding to a formation temperature of 144 ± 2 °C (Table S2). The standard deviation of these values (0.014 ‰) is in excellent agreement with the shot-noise limit of a single analysis, which suggests that the crystal aggregate used for the heating experiments is homogeneous in Δ_{47}. Because this starting value is only ~0.150 ‰ above equilibrated compositions at the temperatures of the heating experiments, 3–7 replicate analyses of each experimental product were typically run in order to determine their Δ_{47} values to useful precision. In total, 128 individual analyses of dolomite powders from heating experiments were made (Table S3). Mean values and 1σ standard errors of replicate analyses are reported in Table 1. Mean Δ_{47} values across all measurement sessions of carbonate standards Carrara Marble and TV03 were 0.414 ± 0.023 (1σ s.d., n = 60) and 0.729 ± 0.021 ‰ (1σ s.d., n = 58), respectively. No significant variations in the mean Δ_{47} values of these standards among separate measurement sessions were observed, and the mean values of these standards are in excellent agreement with published values (e.g., Dennis et al., 2011), so no secondary corrections were applied.

Within every temperature series, Δ_{47} values decrease with time and asymptotically approach the equilibrium values predicted by the Schauble + Bonifacie Δ_{47}–T equation. The time required to reach equilibrium is inversely proportional to the temperature of the experiment: at 717 °C, dolomite Δ_{47} compositions are indistinguishable from equilibrium within five minutes (within 2 s.e.), whereas at 511 °C, apparent equilibration is not observed until 160 hours. The terminal Δ_{47} value in the 486 °C series is barely resolved from equilibrium after 455 hours. Although significant changes in Δ_{47} values occur in the two coldest series (409 and 460 °C), equilibrium is not reached over the timescales of the experiments. Qualitatively similar behavior is observed when equilibrium Δ_{47} values are calculated using the other two T–Δ_{47} calibrations.

Dolomite Δ_{47} values for every temperature–time point are lower than or indistinguishable (within 2σ standard errors) from the preceding time point, with one exception: the mean Δ_{47} value of the penultimate time point in the 614 °C series (t = 4.067 hrs, n = 7) is ~0.027 ‰ above the mean value after 3 hrs (n = 3) of heating at the same temperature. Due to the small 1σ standard errors on these two points (0.005 and 0.003 ‰), the 4 hr time point appears to be resolvably higher in Δ_{47} than the 3 hr time point. A likely cause is minor contamination by foreign carbonate with a high Δ_{47} value. Indeed, this aberrant sample has the lowest $\delta^{13}C$ and $\delta^{18}O$ values among all heating experiments, both of which are beyond two standard deviations from the means of the $\delta^{13}C$ and $\delta^{18}O$ values of all other heating experiments. Because these three independent lines of evidence suggest that the

dolomite from the 4 hr, 614 °C experiment is contaminated (anomalously high Δ_{47} value, anomalously low $\delta^{13}C$ and $\delta^{18}O$ values), we omit this time point from all subsequent analyses.

4. Extracting dolomite Δ_{47} reordering rate constants from experimental data

Here we describe our approach to fitting these dolomite Δ_{47} reordering data with a variety of kinetic models. We first demonstrate that as with calcite and apatite, dolomite clumped isotopic re-equilibration is inadequately described by a single first-order (Arrhenian) rate equation. Then, given no *a priori* reasons for preferring either model, we fit our data using two published non-first order clumped isotope reordering models, describing minor modifications to the models as necessary. In Section 5, we use the results of these models in the context of external constraints to argue for the preference of one of the two.

4.1 A strategy for fitting noisy dolomite Δ_{47} reordering data

The typical procedure for deriving Arrhenian parameters from experimental data is: 1) observe the progress of a reaction at a single temperature in order to derive a reaction rate constant (k) for that temperature; 2) repeat 1) at a handful of temperatures, ideally over the largest possible range where substantial reaction progress can be observed on laboratory timescales; 3) fit a linear line to the derived rate constants in a plot of ln(k) vs. 1/T (i.e., an Arrhenius plot). For a reaction that obeys a first order Arrhenian equation, the rate constant at a given temperature is:

$$k = K_0 e^{-Ea/(RT)} \quad (4)$$

where E_a is the activation energy (usually reported in kJ/mol), K_0 is the pre-exponential factor (in s^{-1}), R is the universal gas constant (= 8.314 J mol^{-1} K^{-1}), and T is temperature (in K). Thus for a linear fit on an Arrhenius plot, the slope of the line is equivalent to E_a/R, and the intercept is the natural log of K_0. Even when reaction progress does not conform to a single first-order rate law, this general approach can still be employed. For example, in the exchange-diffusion model of Stolper and Eiler (2015), calcite Δ_{47} reordering is described by the interplay of two reaction mechanisms, one for the exchange of neighboring carbonate groups, and another for the diffusion of carbonate groups through the crystal lattice. Although the differential equations describing the relationship between the two mechanisms that are used to fit any single temperature–time series are relatively complex, the output of this model is two independent rate constants, one for exchange and one for diffusion, at the temperature of the experiments. By repeating this exercise at other temperatures, the rates of the exchange and diffusion reactions can be described by separate Arrhenius parameters derived from linear fits to separate lines.

Our dataset is poorly suited for extraction of Arrhenian parameters by the above procedure for two reasons: 1) the initial Δ_{47} value of our optical-quality dolomite is ~0.150 ‰ lower than those of optical calcites used in previous studies (Passey and Henkes, 2012; Stolper and Eiler, 2015). This low starting Δ_{47} value halves the Δ_{47} range over which reordering can be observed, so the analytical

uncertainties of individual Δ_{47} measurements have outsized importance and must be explicitly considered in the fits. 2) And, the full range of reaction progress is observed over a relatively limited range of temperatures (486–614 °C) on laboratory timescales (i.e., tens of minutes to hundreds of hours), because outside this range the reaction proceeds too rapidly to observe or too slowly for substantial change to occur. In order to incorporate 'incomplete' reaction progress curves from data generated outside this range into the fits, we departed from the data processing strategies used in previous calcite and apatite reordering studies and instead developed custom global least-squares minimization routines to fit all available Δ_{47} data simultaneously. To observe the sensitivities of these fits to the underlying data, we ran iterative Monte Carlo simulations whereby individual Δ_{47} values were randomly resampled from normal distributions defined by their measured Δ_{47} values and analytical uncertainties. We used the distributions of families of parameters from these iterations to calculate true ideal reordering parameters, the uncertainties on them, and observe correlations among them. We describe our models, and evaluate their success, below.

4.2 A first-order reordering model

Although neither calcite nor apatite Δ_{47} reordering could be adequately fit with a first-order Arrhenian reaction model, it is worth considering whether dolomite can. We thus attempted to fit our data using the first-order model derived in Passey and Henkes (2012). Here, the reaction progress variable is defined as:

$$F = (\Delta_{47,\mathrm{init}} - \Delta_{47,\mathrm{t}})/(\Delta_{47,\mathrm{init}} - \Delta_{47,\mathrm{equil}}), \quad (5)$$

where $\Delta_{47,\mathrm{t}}$ is the mean measured Δ_{47} value of a given heating experiment at a given time, $\Delta_{47,\mathrm{equil}}$ is the clumped isotope composition in equilibrium with the temperature of that experiment, and $\Delta_{47,\mathrm{init}}$ is the mean initial (unheated) composition of the material, 0.452 ‰ (Eqn. A12, Passey and Henkes, 2012). Note that for this model and all subsequent ones, we do not consider the effect of varying $\Delta_{47,\mathrm{init}}$ within its uncertainty envelope on resulting fits because this uncertainty is small (1σ s.e. = 0.002‰) and does not significantly contribute to the value of F. Over the limited range of clumped and bulk compositions measured here, the rate law for Eqn. 1 can be approximated as (c.f. Appendix A, Passey and Henkes, 2012):

$$\frac{\Delta_{47,t} - \Delta_{47,equil}}{\Delta_{47,init} - \Delta_{47,equil}} = e^{-kt}. \quad (6)$$

So, by combining Eqns. 4, 5, and 6, we can derive a simple relationship between a measurable reaction progress variable (F) and the fundamental Arrhenian parameters governing its rate:

$$\ln[1 - F] = -tK_0 e^{-E_a/RT}, \quad (7)$$

which can be expanded using the definition of F to:

$$\Delta_{47,t} = e^{-tK_0 e^{-E_a/RT}} \times \left(\Delta_{47,init} - \Delta_{47,equil}\right) + \Delta_{47,equil} \,. \quad (8)$$

With two unknowns (K_0 and E_a), Eqn. 8 makes an explicit prediction for the Δ_{47} value resulting from heating our dolomite fragment at a single temperature for a prescribed length of time. Thus, we can use a least-squares algorithm to find the ideal K_0 and E_a values that minimize the cumulative differences between predicted and mean measured Δ_{47} values for all thirty heating experiments simultaneously. Note that although one could instead minimize the differences between measured and predicted ln[1–*F*] values using Eqn. 7, as Passey and Henkes (2012) and Henkes et al. (2014) do, we choose not to because such an approach severely over-weights small discrepancies between data and model at large values of F. This is especially problematic because, as clumped isotope compositions closely approach equilibrium, ln[1–*F*] values are particularly sensitive to external factors, such as the choice of Δ_{47}–T calibration used to predict $\Delta_{47,equil}$ values. Although these biases can be somewhat compensated for by propagating analytical uncertainties into ln[1–*F*]-space and employing an error-weighted least-squares algorithm, we find that it is more intuitive and accurate (with respect to internal and external uncertainties) to fit our data in the same reference frame that they were acquired.

We implemented this approach using the *leastsq* algorithm from the *scipy.optimize* module in Python 2.7 to minimize differences between measured and predicted $\Delta_{47,t}$ values according to Eqn. (8). Optimal values for K_0 and E_a were $6.38*10^{11}$ s^{-1} and 250 kJ/mol. Repeating the exercise while weighting residuals by the inverse squares of the 1σ standard errors of mean Δ_{47} values yielded similar results: $4.30*10^{12}$ s^{-1} and 264 kJ/mol. No attempt was made to estimate the uncertainties on these values because it is clear from comparison of experimental Δ_{47} data and predicted Δ_{47} reordering curves using these values that the fits are poor (Fig. S2). Although this simple model adequately agrees with data for high-temperature experiments (at 563 °C, 614 °C, and 717 °C), it is incapable of capturing the more complex reordering behavior evident in the experiments run at lower temperatures. For the 511 °C series, the model severely underestimates the amount of early Δ_{47} reordering that occurs within 1 hr (by about 0.04 ‰) and predicts complete re-equilibration within 65 hours, despite the fact that the datum at this time is resolved from equilibrium by ~0.04 ‰ (Fig. 1). The failure of the first-order model is especially obvious at 460 °C: in order to accommodate a net decrease in Δ_{47} of 0.075 ‰ after 86 hours, the first-order model is forced to fully equilibrate, and lower in Δ_{47} by another 0.058 ‰, within ~300 hours. However, the agreement (within uncertainty) of the Δ_{47} values of 460 °C experiments at 86 and 314 hours suggests that no detectable reordering occurred over this time interval. It is clear that as with calcite and apatite, dolomite Δ_{47} reordering is inadequately described by first-order kinetics. Instead, a more complex, non first-order model is required to fit these data.

4.3 The transient defect/equilibrium defect model

To account for the initially-rapid Δ_{47} reordering that is observed in their experiments, Henkes et al. (2014) invoke an additional, transient reordering mechanism with the rate constant k_d, whose contribution to the net reordering rate declines by a temperature-dependent exponential decay rate k_2. The physical grounding for this model is described in Section 1.2. Mathematically, this approach amounts to adding an additional term to Eqn. 6 whose relative size decays with time (Henkes et al., 2014):

$$\ln\left(\frac{\Delta_{47,t}-\Delta_{47,equil}}{\Delta_{47,init}-\Delta_{47,equil}}\right) = -k_c t + \frac{k_d}{k_2}\left(e^{-k_2 t}-1\right). \quad (9)$$

Note that here, k_c is equivalent to the k term in the previous section, and represents the rate constant for invariant reordering governed by the equilibrium defect concentration. Each of these three rate constants is described by an independent Arrhenius equation, so the full, ten-parameter equation describing Δ_{47} as a function of time becomes:

$$\Delta_{47,t} = e^{-tK_c e^{-E_c/RT}} \times e^{\frac{K_d e^{E_d/RT}}{K_2 e^{E_2/RT}} \times \left[e^{-tK_2 e^{E_2/RT}}-1\right]} \times \left(\Delta_{47,init}-\Delta_{47,equil}\right)+\Delta_{47,equil}. \quad (10)$$

This equation has six unknowns—i.e., pre-exponential factors and activation energies for each of the three rate constants: the equilibrium defect component (k_c), the transient defect component (k_d), and the annealing rate of the transient defect component (k_2). Analogous to the procedure described in Section 4.2, we use the *scipy.optimize leastsq* global least squares minimization algorithm to fit Eqn. 10 for all thirty data points and derive optimal Arrhenius parameters for the three rate constants.

This procedure finds reasonable values for all six parameters, which can be used to generate reordering curves that adequately describe the data (Fig. 1, Table 2). Initial attempts to fit these data while weighting each Δ_{47} value by the inverse square of its 1σ standard error produced unreasonable, negative values for the activation energies of k_d and k_2. This occurred because small residuals on a few data points with unusually small standard errors (e.g., 1σ std. errors of three points are 0.003 ‰) were greatly over-weighted by the fit penalty function at the expense of all other points. To compensate for this, while still weighting data points proportional to their uncertainties, we imposed an upper limit on the weight of any data point determined by the reciprocal of the shot noise-limited variance given by the expected standard error of a single measurement (0.017‰) and the square root of the number of replicates. We estimated the true uncertainties on these 'best fit' Arrhenius parameters using an iterative Monte Carlo scheme. For each iteration the following sequence was performed: 1) each of the 121 individual Δ_{47} measurements were resampled from normal distributions defined by their mean Δ_{47} values and standard measurement errors using 121 independent, true random number generators; 2) mean Δ_{47} values for all thirty experiments were re-computed from

the new values generated in step 1); 3) new optimal Arrhenius parameters were generated by fitting Eqn. 10 to this iteration's mean Δ_{47} values using the same least-squares algorithm described above.

We repeated this procedure for 10,000 iterations, recording the set of six Arrhenius parameters generated in each one. Histograms of each parameter, and covariances among them for the 10,000 evaluations are shown in Fig. S3. Distributions are approximately Gaussian. Minor secondary aberrations in the histograms of $\ln(K_d)$, E_d, $\ln(K_2)$, and E_2, however, suggest that a small minority of the iterations produced families of parameters with distributions that are offset from, but largely overlap with, the dominant Gaussian populations. Given no *a priori* reason for preferring one population of fits to another, we report the mean values and standard deviations of the entire data set as conservative estimates of the most likely Arrhenius parameters and the uncertainties on them (Table 2). This full Monte Carlo uncertainty estimation procedure was repeated for all three Δ_{47}–T calibrations.

It is well established but rarely acknowledged that uncertainties on paired Arrhenius parameters are highly correlated (Héberger and Kemény, 1987; Nagy and Turányi, 2011). Since such correlations have direct bearing on the application of carbonate Δ_{47} reordering models (e.g., Lloyd et al., 2017), it is worth considering how the families of dolomite Δ_{47} reordering parameters covary here. It is evident from cross-plots of the Monte Carlo evaluations of the six parameters that they fall into two groups (Fig. S3). Pearson correlation coefficient matrices of these families of parameters bear this out as well (Tables S4–S6). $\mathrm{Ln}(K_c)$ and E_c are positively correlated (r^2 of 0.277 to 0.991, depending on the Δ_{47}–T calibration), but not correlated with any other parameters. Arrhenius parameter pairs $\ln(K_d)$ and E_d, and $\ln(K_2)$ and E_2 are similarly well-correlated (r^2 of up to 0.992 and 0.987, respectively), and in addition, all four parameters have significant correlations between them (r^2 of 0.262 to 0.922). These correlations provide useful guidelines for how to apply the uncertainties listed in Table 2 to reordering models. For the first-order approximation model (i.e., solely considering Δ_{47} reordering due to unannealable defects), reasonable estimates of 1σ confidence intervals can be found by jointly varying mean values of $\ln(K_c)$ and E_c by their 1σ standard deviations (Table 2). The lack of an analytical solution to Eqn. 10 precludes application of the full transient defect/equilibrium defect model to anything other than isothermal temperature-time paths (Henkes et al., 2014). Nonetheless, uncertainties on rate constants for such scenarios should be propagated by perturbing $\ln(K_d)$, E_d, $\ln(K_2)$, and E_2 jointly by equal proportions of the standard deviations on their mean values. The effects of Arrhenius parameter uncertainties on predictions for the susceptibility of dolomite Δ_{47} to reordering are evaluated in a later section.

4.4 A dolomite exchange-diffusion reordering model

A second model that successfully accounts for the non-first order Δ_{47} reordering behavior observed during heating experiments was developed by Stolper and Eiler (2015). Rather than relying on the annealment of defects to account for decreasing

reordering rate with time, they use a model that explicitly accounts for the formation and destruction of multiply-substituted 'clumped' carbonate groups through isotope exchange among adjacent, singly-substituted groups ('pairs'). Here, the two-stage reordering occurs because complete re-equilibration is initially buffered against by a high concentration of pairs that persist adjacent to previous clumped carbonate groups until further heating causes these pairs to be diffused away as singletons. The reaction progress parameter, ξ, here tracks the concentration of clumped isotopologues with time, from an initial concentration ($[^{13}C^{18}O^{16}O_2^{2-}]_0$) to a final concentration in equilibrium with the reaction temperature ($[^{13}C^{18}O^{16}O_2^{2-}]_{eq}$). This reaction progress parameter is related to the Δ_{47} value by:

$$\Delta_{47} = \left(\frac{[^{13}C^{18}O^{16}O_2^{2-}]_0 - \xi}{[^{13}C^{18}O^{16}O_2^{2-}]^*} - 1 \right) + \Delta_{47,\,T=\infty} \quad , \qquad (11)$$

where $[^{13}C^{18}O^{16}O_2^{2-}]^*$ is the concentration of the primary multiply-substituted species given a stochastic distribution of ^{13}C and ^{18}O, and $\Delta_{47,T=\infty}$ is the theoretical Δ_{47} value at infinite temperature (0.259–0.268 for the T–Δ_{47} calibrations employed in this study; note that in Eqn. 11 the actual value of $\Delta_{47,T=\infty}$, not reported permil notation, is used). This approximation ignores the contribution of other isotopologues at cardinal mass 47, which is reasonable for typical carbonate compositions given the analytical uncertainty on Δ_{47} values (Wang et al. 2004). With a few simplifications described in Stolper and Eiler (2015), the derivative of reaction progress at a given time, t, can be defined as:

$$\frac{d\xi}{dt} = k_f \times [^{12}C^{16}O_3^{2-}] \times \left([^{13}C^{18}O^{16}O_2^{2-}]_0 - \xi \right) - k_f \times \frac{[^{12}C^{16}O_3^{2-}] \times [^{13}C^{18}O^{16}O_2^{2-}]_{eq}}{[pair]_{eq}} \times [pair]_t \quad , \qquad (12)$$

where the corresponding time-dependent pair concentration is governed by:

$$\begin{aligned} \frac{d[pair]_t}{dt} = {} & k_f \times [^{12}C^{16}O_3^{2-}] \times \left([^{13}C^{18}O^{16}O_2^{2-}]_0 - \xi \right) - k_f \times \frac{[^{12}C^{16}O_3^{2-}] \times [^{13}C^{18}O^{16}O_2^{2-}]_{eq}}{[pair]_{eq}} \times [pair]_t \\ & + k_{diff,single} \times [^{13}C^{16}O_3^{2-}] \times \left(1 - [^{12}C^{18}O^{16}O_2^{2-}]\right)^z \times [^{12}C^{18}O^{16}O_2^{2-}] \times \left(1 - [^{13}C^{16}O_2^{2-}]\right)^z \\ & - k_{diff,single} \times \frac{[^{13}C^{16}O_3^{2-}] \times \left(1 - [^{12}C^{18}O^{16}O_2^{2-}]\right)^z \times [^{12}C^{18}O^{16}O_2^{2-}] \times \left(1 - [^{13}C^{16}O_2^{2-}]\right)^z}{[pair]_{eq}} \times [pair]_t \end{aligned} \qquad (13)$$

In this set of differential equations, the three unknowns are k_f, $k_{diff,single}$, and $[pair]_{eq}$, representing the rate constant for exchange between 'pairs', the rate

constant for diffusion of singletons through the crystal lattice, and the concentration of pairs at equilibrium, respectively. *z* is the number of adjacent carbonate groups in the unit cell (6 for dolomite as well as calcite). Concentrations of singly-substituted species are treated as constants and calculated directly from the mean $\delta^{13}C$ and $\delta^{18}O$ values of the crystal. As Stolper and Eiler (2015) did, we initially assumed that the pair concentration at high-temperature equilibrium was indistinguishable from a stochastic configuration of singly-substituted species distributed throughout the crystal lattice, calculated as:

$$[\text{pair}]_{\text{rand}} = \frac{[^{13}C^{16}O_3^{2-}] \times \left(1 - \left(1 - \left[^{12}C^{18}O^{16}O_2^{2-}\right]\right)^z\right) + [^{12}C^{18}O^{16}O_2^{2-}] \times \left(1 - \left(1 - \left[^{13}C^{16}O_2^{2-}\right]\right)^z\right)}{2}$$

(14)

We additionally assumed that the rate constants k_f and $k_{diff,single}$ conform to the Arrhenius equation, so at any temperature their values can be derived from independent pairs of E_a and K_0 (Eqn. 4). We can thus solve the system of Eqns. 12 and 13 using the *scipy.integrate.odeint* wrapper for the *lsoda* ODE solver to predict ξ and [pair] at every experimental temperature-time point, given global values for these four Arrhenius parameters: $\ln K0_f$, Ea_f, $\ln K0_{diff,single}$, $Ea_{diff,single}$. Residuals between measured Δ_{47} values and those predicted by ξ and Eqn. 11 can thus be fed to the error-weighted *scipy.optimize leastsq* global least squares minimization algorithm in order to find optimal values for $\ln K0_f$, Ea_f, $\ln K0_{diff,single}$, $Ea_{diff,single}$.

Integrating Eqs. 12 and 13 to any time point requires initial values for ξ and [pair]. Initial reaction progress is 0 by definition, but the proper initial concentration of pairs is less intuitive. As with the Stolper and Eiler (2015) model and the reaction-diffusion model for OH and H_2O in silicates model upon which the former is based (Zhang et al., 1995), we find that initializing this dolomite Δ_{47} reordering model with a random distribution of pairs results in a poor fit to the data. Stolper and Eiler (2015) find the best fit to their calcite Δ_{47} data when $[\text{pair}]_0$ is 0.030 ‰ larger than $[\text{pair}]_{\text{rand}}$. They hypothesize that this pair excess is the result of an equilibrium pseudo-secondary isotope effect that preferentially pairs singly-substituted carbonate groups when the calcite crystal is precipitated at 55 °C. Using this optimal $[\text{pair}]_0$, the pair concentration at the end of the 430 °C run, and the assumption that no preference exists at the high temperature limit, they propose the equation:

$$\ln\left(\frac{\left[\text{pair}\right]_{\text{eq}}}{\left[\text{pair}\right]_{\text{rand}}}\right) = \frac{m_p}{\text{T}}, \qquad (15)$$

where m_p = 0.0992, to calculate the equilibrium pair concentration as a function of calcite bulk composition (from Eqn. 14) and temperature (in Kelvin). Model fits of

our dolomite Δ_{47} data using this value for m_p in Eqn. 15 and the formation temperature of our material (144 °C) fail to capture the 'kinks' in the reaction progress curves. This failure is due to an overabundance of initial pairs that increases the rate of the clump-forming back reaction, which obscures the 'rapid' reordering stage that must initially occur. A new m_p must be found for dolomite, but the optimal initial and equilibrium pair concentrations, which depend on m_p, are codependent on the optimal rate constants for exchange and diffusion for any solutions to Eqns. 12 and 13. To account for this possibility, we introduced m_p as another free parameter for our fits, and used this parameter along with Eqn. 15 to calculate $[\text{pair}]_{eq}$ for every experimental temperature and the initial pair concentration for the formation temperature. We then used our global least squares algorithm to minimize the difference between mean measured and predicted Δ_{47} values for five independent parameters: $\ln(K0_f)$, Ea_f, $\ln(K0_{diff,single})$, $Ea_{diff,single}$, and m_p.

Results of the error-weighted least squares fit are reported in Table 3, and shown in Fig. 2. The optimal value for m_p is markedly different from that of calcite: 0.0663 to 0.0785 (depending on calibration choice) vs. 0.0992, which results in approximately two-thirds of the predicted equilibrium pair excess at the same temperature. This discrepancy is not inherently problematic. Calcite and dolomite have different temperature sensitivities to a variety of equilibrium isotope effects; indeed, such discrepancies are the foundation for a variety of thermometers, including the dolomite–calcite ^{18}O and ^{13}C inter-mineral exchange thermometers (Sheppard and Schwarcz, 1970). Since this apparent pair excess is hypothesized to represent a pseudo-secondary isotope effect by which the net free energy of a crystal lattice is lowered when heavy isotope-bearing carbonate groups are preferentially paired, it is reasonable to expect that the different lattice dimensions and compositions of different minerals would result in different temperature sensitivities to this hypothesized effect.

As with the transient defect/equilibrium defect model, we used a Monte Carlo scheme to observe the dependence of the fitted parameters ($\ln K0_f$, Ea_f, $\ln K0_{diff,single}$, $Ea_{diff,single}$, and m_p) on the analytical uncertainties on the values underlying the mean Δ_{47} data. As in Section 4.3, we independently varied the raw Δ_{47} values by their uncertainties and re-fit the resulting data for 10,000 iterations. We then used the distributions of acceptable fits to observe the uncertainties on and correlations among the five parameters.

Mean Arrhenius parameters (and m_p) for the Monte Carlo simulations are extremely similar to those of the best fit to the measured data for each Δ_{47}–T calibration (Table 3). Distributions of individual parameters are approximately gaussian, suggesting that the standard deviations of these distributions are appropriate estimates of the totals uncertainties on these parameters (Fig. S4). Mean kinetic parameters for all three calibrations agree within uncertainty (Table 3). However, when used to forward-model dolomite Δ_{47} reordering and compare to natural data, the discrepancies in the three calibrations in the range of ~300–800 °C result in resolvably-different Δ_{47} values for scenarios involving such elevated

conditions (see below). As with the transient defect/equilibrium defect parameters, corresponding pairs of Arrhenius parameters for exchange and diffusion rates are strongly correlated (Pearson r^2 values for exchange and diffusion components are 0.835 and 0.987, respectively), but only moderately correlated between mechanisms (r^2 of, at most, –0.106) (Tables S7–S9). Accordingly, we suggest covarying pairs of Ea and lnK0 for each rate constant when applying these parameters to forward reordering models, and only covarying paramaters across components in accordance with the correlations reported in Table S4. m_p values are inconsistently correlated with any of the four Arrhenius parameters (r^2 = –0.242 to 0.341), which suggests that fits are not sensitive to the exact m_p value chosen. If so, it is reasonable to fix m_p to its mean value (0.0720) in forward models.

5 Discussion

Here we compare our dolomite Δ_{47} reordering parameters to previously published parameters for calcite. We use trends among these parameters and external constraints to suggest that the exchange-diffusion model more closely approximates the mechanism for the non-first order reordering behavior observed in all carbonates. We then use forward models and these favored Arrhenius parameters to predict Δ_{47} values of dolomites in a variety of geologically-relevant scenarios, and discuss the implications for preserving original dolomite Δ_{47} compositions and constraining the thermal histories of deeply-buried sediments.

5.1 Assessing the agreement with dolomite marbles

Any reasonable model for dolomite Δ_{47} reordering must be able to reproduce the apparent equilibrium blocking temperatures measured in cooled metamorphic terranes. Dolomite Δ_{47} temperatures in high-grade marbles range from 250 to 450 °C, and broadly correlate with cooling rate: colder clumped isotope temperatures are found in slowly-cooled dolomite marbles from orogenic belts (e.g., del Real et al., 2016), while the hottest dolomite Δ_{47} temperatures are found in the contact aureoles from shallow plutonic intrusions (Ferry et al., 2011; Lloyd et al., 2017). We compared these values to those predicted by dolomite Δ_{47} reordering models during linear cooling from high temperature (Fig. 3). Briefly, we initialized reordering models with dolomite Δ_{47} values and pair concentrations in equilibrium at 600 °C, and held them at this temperature for 10^5 years. Then, we cooled the system from 600 to 0 °C at fixed rates between 10^0 and 10^6 °C/Ma. For all three Δ_{47}–T calibrations, we modeled the changes in Δ_{47} values on these temperature-time paths using the exchange-diffusion model (Fig. 3) and the unannealable (equilibrium) component of the transient defect/equilibrium defect model (Fig. S5), and the corresponding parameters for these models determined above. We estimated the uncertainties on the predictions of the first-order equilibrium defect model by co-varying pairs of $\ln(K_c)$ and E_c by the same proportion of their standard deviations and repeating the modeling exercise. The final predicted Δ_{47} values from the exchange-diffusion model were comparably sensitive to uncertainties on the rate constants for the exchange and diffusion components, but the rate constants for these two components are inconsistently correlated with each other (Tables S7–S9).

So, we sequentially perturbed the Arrhenius parameters for the two components in separate model runs and report the values most different from the mean value at every time point. This approach is the most conservative estimate of the net effect of uncertainties on the predicted apparent equilibrium blocking temperatures for dolomite marbles.

For both types of models and all Δ_{47}–T fits, modeled apparent equilibrium blocking temperatures increase with increasing cooling rate (Figs. 3, S5). For the first-order approximation to the transient defect/equilibrium defect model, results of all three Δ_{47}–T calibrations agree within uncertainty, however the uncertainties on the predicted blocking temperatures are large enough (up to ~0.100 ‰ at low cooling rates) that these parameters are functionally useless for constraining the thermal histories of dolomitic marbles (i.e., geospeedometry) (Fig. S5). The large uncertainties derived from Monte Carlo perturbations of the transient defect/equilibrium defect model may suggest that this model is poorly suited for approximating clumped isotope reordering in dolomite.

Uncertainties on the exchange-diffusion models, on the other hand, are small enough that meaningful differences in the results of the three Δ_{47}–T calibrations can be resolved and discussed. With the Bonifacie and Lloyd calibrations, predicted Δ_{47}-derived temperatures are moderately but notably colder than those measured in most slowly-cooled dolomite marbles (Fig. 3). For instance, the exchange-diffusion model predicts apparent equilibrium temperatures of between 200 and 260 °C (2σ) for exhumation/cooling rates between 10 and 100 °C/Ma. And, apparent equilibrium blocking temperatures at or above 300 °C require exhumation rates in excess of ~10,000 °C/Ma. Directly comparing these predictions to observed Δ_{47} values from exhumed metamorphic terranes is challenging because precise constraints on the cooling rates at these relatively low temperatures are uncommon, and processes related to exhumation such as strain-induced recrystallization tend to disperse Δ_{47} values and obscure primary reordering signals (Ryb et al., 2017). Comparisons with dolomite marbles from contact aureoles are more straightforward, although not necessarily more accurate, because their T-t paths can be estimated with conductive cooling models built for the geometry of specific intrusions (Lloyd et al., 2017). Nonetheless, we note that only the Lloyd-calibrated dolomite Δ_{47} reordering model agrees with measured values from the Notch Peak aureole (Lloyd et al., 2017), and then only at the slowest reordering rates permitted by the 2σ uncertainty envelope. Neither model is capable of reproducing the exceptionally low Δ_{47} value of the Predazzo aureole ($\Delta_{47,ARF}$ = 0.327 ± 0.023 ‰; from Ferry et al. (2011), but projected into the ARF using the transfer function of Ryb et al. (2017)).

On the other hand, with the Schauble + Bonifacie calibration, acceptable agreement between natural dolomites and the exchange-diffusion model is observed for both regionally-metamorphosed and contact-metamorphosed settings (Fig. 3). The predicted apparent equilibrium blocking temperatures for all three calibrations agree within uncertainty (Tables S10–S12). In Δ_{47}-space, however, the

Schabule + Bonifacie calibration diverges to lower Δ_{47} values. This discrepancy occurs because Δ_{47}-derived temperature estimates in the realm of 250–450 °C are especially sensitive to the choice of calibration curve and minor (< 0.01‰) analytical artifacts, a persistent challenge of the technique (e.g., Huntington et al., 2009; Dennis et al., 2011; Daëron et al., 2016). In fact, this temperature range is also where equilibrium dolomite Δ_{47} values are least well constrained: Δ_{47} values of synthetic dolomites grown at 302 and 351 °C disagree with predictions from the T–Δ_{47} calibration used in this study by 0.014 and 0.033 ‰, respectively (Bonifacie et al., 2017). Thus, these significant discrepancies indicate that dolomite clumping in the range of 250–450 °C is still incompletely understood, and could explain the apparent disagreement between our models and others' measurements. Because the Schauble-derived parameters agree better, we recommend using these values and this calibration, and exclusively consider models built on these values for the remainder of this study. On the other hand, given the variations in the structural characteristics of natural dolomites, it is possible that the reordering parameters determined for the Eugui dolomite formed from hydrothermal fluid in an open fissure are not applicable to coarse, granoblastic dolomite fabrics formed under stress in regionally-metamorphosed sections. Additional heating experiments, with a different starting material, would be needed to address this possibility.

5.2 Comparisons with calcite reordering parameters

Arrhenius plots of derived dolomite Δ_{47} reordering parameters can be used to directly compare these values with those of calcite, and consider whether trends in these parameters are consistent with expectations for the hypothesized mechanisms behind the two reordering models (Figs. 4, 5). We first consider the parameters of the exchange-diffusion model because their interpretation is more straightforward. Arrhenius parameters for dolomite are larger than calcite for both components, but more dissimilar from calcite with respect to the diffusion of singletons. At temperatures below ~700 °C, dolomite reordering is generally slower than calcite, and this behavior is present in both components (Fig. 4). At 700 °C and above, the rates of isotopic exchange between pairs and diffusion of singletons in dolomite and are indistinguishable. In extrapolations to temperatures below 400 °C, the rates of both mechanisms in calcite and dolomite diverge. This behavior is consistent the compensation (Meyer-Neldel) rule—i.e., the empirical phenomenon that activation energies and pre-exponential factors of related chemical processes are typically correlated (e.g., Yelon et al., 1992). A consequence of this effect is that the rates of chemical processes with a shared mechanism, such as the diffusion of species through similar crystal structures, tend to diverge at low temperatures and converge at a high temperature (Brady and Cherniak, 2010; Farver, 2010). The diffusivities of different elements in carbonates have an unusually strong adherence to the compensation rule (r^2 = 0.97; Brady and Cherniak, 2010), perhaps due to their simple stoichiometry and similar crystal structures. Experimental data for carbonates other than calcite are limited, but suggest that diffusivities of the same species are systematically slower in dolomite (Anderson, 1972). This ordering is consistent with the predictions of the anion porosity model of Zheng and Fu (1998),

wherein the tighter packing of anions in dolomite unit cells results in increases in the activation energy and pre-exponential factor for oxygen self-diffusion in this phase. Of course, oxygen-self diffusion in carbonates and the singleton diffusion component of clumped isotope reordering are not equivalent processes; indeed, the rates of these two processes are different in natural systems (Lloyd et al., 2017), and the former is strongly dependent on f_{H2O} while a dependence in the latter has not yet been observed outside of uncertainty (Passey et al., 2012; Brenner et al., 2018). Instead, we merely note that the order of Δ_{47} reordering rates in calcite, dolomite, and magnesite suggested by the apparent equilibrium blocking temperatures in natural carbonates (del Real et al., 2016; Lloyd et al., 2017), and corroborated by this study, is consistent with the ranking of ion porosities in these three related phases (Fortier and Giletti, 1989; Zheng and Fu, 1998). Moreover, it is noteworthy that the isokinetic temperature for elemental diffusion in carbonates—i.e., the temperature at which diffusivities of all species converge—is 690 °C (Brady and Cherniak, 2010), which is in good agreement with the temperature at which $k_{diff,single}$ in calcite and dolomite are indistinguishable (~700°C; Fig. 4). This is further, albeit circumstantial, evidence that the physical process represented by $k_{diff,single}$ may be comparable to atomic-scale diffusion through the crystal lattice. By the same logic, it is perhaps unsurprising that the rates of pair exchange in calcite and dolomite are so similar. If k_f represents the rate of exchange of ^{18}O atoms between neighboring carbonate groups, its primary control should be the strength of the C–O bond. This C–O bond strength should be similar in all carbonates, and relatively insensitive to second-order effects such as the spacing of carbonate groups and the ionic strength of the local cations (Cole and Chakraborty, 2001).

Above, we showed that Arrhenius parameters for the exchange-diffusion model generally adhere to expected trends for chemical processes such as diffusion and isotopic exchange. In contrast, Arrhenius parameters for the transient defect/equilibrium defect model depart from similar expectations. Although the activation energy for the equilibrium defect component in dolomite is indistinguishable from optical calcite or brachiopod calcite, the dolomite pre-exponential factor is lower than the two calcites (Henkes et al., 2014). Unusual trends are also apparent from the Arrhenius plots of the other two components (Fig. 5): rate constants for transient defect reordering and the annealing rate of these defects diverge at high temperatures, and converge, if at all, at temperatures less than 400 °C. It is reasonable to expect that defect concentration, and perhaps defect style, would be idiosyncratic to each carbonate grain and its formation environment (Passey and Henkes, 2012). It is more surprising that the concentration-normalized annealing rate is not an intrinsic property of a mineral. The progressive annealing of defects in carbonates has been invoked previously to explain the anomalously-rapid, time-dependent self-diffusion rate of oxygen in calcite at 550–600 °C (Kronenberg et al., 1984; Farver, 1994). Although the data from these experiments are too sparse to explicitly calculate Arrhenius parameters for this process, it is evident that the annealing rate operates on timescales of hours to days at 550 °C (Farver, 1994). Δ_{47} reordering experiments, however, suggest that calcites are fully annealed with respect to defects at 475 °C in a matter of minutes, and presumably in far less time

at 550 °C (Henkes et al., 2014). Although these annealing rates are merely inferred from observations of the time-dependence of distinct processes that are not directly comparable (see above), the vast differences in rate are still difficult to reconcile. How can calcite be fully annealed with respect to Δ_{47} reordering after an hour at 475 °C, yet completely 'open' to transient defect-assisted ^{18}O diffusion after the same treatment? What physical change occurs in carbonates on hours-to-days timescales at 550 °C, and how does it affect Δ_{47} reordering kinetics? It is not possible to address the latter question with existing clumped isotope reordering datasets because all studied samples are fully or nearly equilibrated with respect to Δ_{47} at this temperature after an hour, but perhaps it will be possible by studying carbonates with slower reordering kinetics (such as, apparently, magnesite (del Real et al., 2016)). The inconsistencies of Arrhenius parameters from this model with expectations for Arrhenian processes suggests that non-first order Δ_{47} reordering behavior is not defect-controlled. In contrast, due to the broad agreement of parameters from the exchange-diffusion model with expected trends in calcite and dolomite, we suggest that this formulation more closely approximates the behavior of carbonate groups in a crystal lattice.

5.3 Implications for recovery of dolomite formation temperatures and peak burial conditions

Dolomite reordering parameters can be used to predict the time-temperature treatments under which dolomite formation conditions can be recovered from ancient buried sections. We first explore the susceptibility of dolomite to reordering during isothermal heating pulses (Fig. 6). In these scenarios, dolomite equilibrated at 25 °C is instantaneously heated to a specified peak temperature, held there for 60 Ma, and then quenched back to 25 °C. Peak temperatures range between 120 and 240 °C. Predicted Δ_{47} values from the mean kinetic parameters for the transient defect/equilibrium defect model and the first-order approximation model are indistinguishable over this range. Both models predict no measureable Δ_{47} reordering when dolomite is held at 150 °C or below. At 180 °C, dolomite Δ_{47}-derived temperatures are partially reordered from 25 °C to ~120 °C after 60 Ma (Table S13). Full re-equilibration occurs at 210 °C and above, but the timescale for re-equilibration is sensitive to the exact peak temperature used: dolomite Δ_{47} values require 60 Ma to fully reorder at 210 °C, but less than 5 Ma to fully reorder at 240 °C. Error envelopes are omitted from Fig. 6 for clarity, but note that propagating uncertainties on the Arrhenius parameters for the equilibrium defect component dramatically shifts the window where dolomite Δ_{47} values are sensitive to specific temperatures. Over a conservative 2σ window of likely pairs of E_c and $\ln K_c$, dolomite Δ_{47} values held at 180 °C for 60 Ma may be fully re-equilibrated with this peak temperature or not reordered at all (Table S13). Likewise, the highest temperature that epigenetic dolomite can be held at for 60 Ma without measurably altering its Δ_{47} value may be as high as 190 °C or lower than 120 °C (within 2σ). Since laboratory experiments at or near these conditions would be impractical, observations of naturally reordered dolomite fabrics in well-

constrained sections may be needed to more precisely calibrate these reordering kinetics.

In contrast to cooling systems where the first-order approximation and exchange-diffusion models give similar predictions, in these isothermal heating scenarios significant differences in the style of predicted dolomite Δ_{47} reordering behavior are apparent. Transient defect/equilibrium defect models predict a single temperature window over which the complete transition from unperturbed to fully-equilibrated Δ_{47} values occur, even if the exact location of this window is highly uncertain. In the exchange-diffusion model, dolomite Δ_{47} reordering during burial occurs in two distinct steps (Fig. 6). Partial re-equilibration occurs on various timescales between 150 and 240 °C (Table S14). Once this partially reordered state is reached, Δ_{47} values are effectively invariant for the remainder of the heat treatment. Full Δ_{47} equilibrium is only approached at higher temperatures, likely at or above 240 °C. This two-phase behavior is a natural consequence of the model construction (Stolper and Eiler, 2015); rapid partial reordering occurs by destruction of $^{13}C^{18}O^{16}O_2^{2-}$ groups through exchange with neighboring carbonate groups containing no rare isotopes. In the temperature realm where singletons are effectively closed to diffusion, this process builds up an excess of pairs that buffer the system against further reordering through the clump-forming back-reaction. Only at higher temperatures is the singleton diffusion rate fast enough to deplete this pair excess and allow complete re-equilibration of the crystal. This same two-phase reordering style is observed in calcite, but at lower temperatures. Because the rates of exchange and diffusion are more disparate in dolomite than calcite, the temperature window in which Δ_{47} values are partially open to reordering is relatively large (~100 °C). Because partially reordered dolomite Δ_{47} values increase monotonically but with alternating concavity, large changes in apparent equilibrium Δ_{47} value can accompany small changes in ambient temperature around an inflection point.

To understand the implications of this nonlinear sensitivity of dolomite Δ_{47} reordering rate to certain temperature windows, we modeled this system in a simple burial-residence-exhumation scenario (Fig. 7). Here, dolomite Δ_{47} was initialized in equilibrium at 50 °C, then heated by burying the system at a rate of 1 mm/yr along a geotherm of 25 °C/km to a depth and peak temperature of 10 km at 250 °C. Dolomite was held at this depth for 5 Ma, and subsequently exhumed to surface conditions at the same rate as burial. Initial dolomite Δ_{47} compositions are scrambled at temperatures similar to those suggested from binary box-car models; dolomite Δ_{47} values likely resist reordering until at least 150 °C. From 150 °C to 200 °C, dolomite Δ_{47} values are partially open to re-equilibration by the exchange mechanism only: a fraction of $^{13}C–^{18}O$ bonds are broken, increasing the excess of pairs that cannot diffuse away until higher temperatures are reached. Above ~200 °C, some amount of additional Δ_{47} re-equilibration is facilitated through singleton diffusion, although the degree and timescale of this re-equilibration is highly uncertain. During cooling and exhumation, some amount of back-reaction to higher Δ_{47} values occurs until ~150 °C. This back-reaction will further deplete the

pair concentration, perhaps even to a value below the concentration in equilibrium at 250 °C. Such behavior illustrates why, even with symmetric T-t paths, carbonate clumped isotope reordering in the exchange-diffusion model can be highly irreversible. In carbonates with natural abundances of ^{13}C and ^{18}O, depletion of initial pair populations through diffusion of singletons during heating at and above ~200 °C is essentially a one-way reaction. This process drastically reduces the capacity of carbonates to re-equilibrate to higher Δ_{47} values during exhumation, causing relatively high apparent equilibrium Δ_{47} temperatures to be preserved. One implication of this behavior is a means to distinguishing between pristine and reordered carbonates with the same Δ_{47} value: a dolomite crystal formed in equilibrium at 200 °C will have an elevated concentration of pairs relative to a dolomite crystal that was heated above 200 °C and partially re-equilibrated to a Δ_{47} value corresponding to this temperature during cooling. Initial experiments designed to infer such differences in pair concentrations by subjecting crystals to additional heat treatments have large analytical uncertainties that make interpretation of the results challenging (Ryb et al., 2017). Further experiments and investigations of appropriate natural materials would be needed to observe differences in pair concentrations with high confidence, but if successful, would strengthen the application of the exchange-diffusion model to carbonate clumped isotope reordering in the solid state.

6 Conclusions

Dolomite Δ_{47} values have great potential for comparing the conditions of dolomitization in ancient carbonate sections to those of the modern, but ancient clumped isotope compositions may be modified by prolonged burial heating in the intervening times. We subjected fragments of a stoichiometric dolomite crystal aggregate to isothermal heating experiments in a cold seal apparatus held at 409 to 717 °C for between 5 minutes and 455 hours to observe the dependence of dolomite Δ_{47} reordering rate on temperature and time. We fit these data to two existing models for carbonate clumped isotope reordering, generating Arrhenius parameters that can be used to predict dolomite Δ_{47} values for any reasonable temperature-time path. Although we prefer the exchange-diffusion model of Stolper and Eiler (2015) to the transient defect/equilibrium defect model of Henkes et al. (2014) because derived parameters for the latter model are less consistent with expected trends among diffusivities in carbonates, both models are capable of reproducing the apparent equilibrium blocking temperatures observed in cooled high-grade dolomites from contact aureoles and regionally metamorphosed terranes (~250–300 °C). The reordering style in simple burial heating scenarios differs markedly between the models, but the models agree that dolomite is likely resistant to reordering of diagenetic Δ_{47} values at ambient temperatures at least as high as 120 °C, and likely up to 150 °C, for geologic timescales.

Acknowledgements

We thank C. Ma and N. Kitchen for assistance with instrumentation and the acquisition of key data for this work. G. Rossman offered suggestions and invaluable assistance in acquiring the dolomite sample. We are grateful to D. Stolper and M. Bonifacie for suggestions that improved this work. This project was funded by NSF EAR Award #1322058 to J.M. Eiler.

Supplementary Materials

Supplementary data tables and figures can be retrieved from the online version of this article. A free, flexible software package for running Δ_{47} reordering models of both calcite and dolomite for any user-specified T-t path is available online and updated regularly at www.github.com/maxmansaxman/Clumpy_reordering_model_distribution.

WORKS CITED:

Anderson, T.F., 1972. Self‐diffusion of carbon and oxygen in dolomite. J. Geophys. Res. 77, 857‐862.

Arvidson, R.S., Mackenzie, F.T., 1999. The dolomite problem; control of precipitation kinetics by temperature and saturation state. American Journal of Science 299, 257–288. doi:10.2475/ajs.299.4.257

Barber, D.J., Heard, H.C., Wenk, H.R., 1981. Deformation of dolomite single crystals from 20–800 C. Phys Chem Minerals 7, 271–286.

Barber, D.J., Reeder, R.J., Smith, D.J., 1985. A TEM microstructural study of dolomite with curved faces (saddle dolomite). Contrib Mineral Petrol 91, 82–92.

Bergmann, K.D., 2013. Constraints on the carbon cycle and climate during the early evolution of animals. PhD Thesis, Caltech.

Blank, J.G., Stolper, E.M., Carroll, M.R., 1993. Solubilities of carbon dioxide and water in rhyolitic melt at 850 C and 750 bars. Earth and Planetary Science Letters.

Blättler, C.L., Miller, N.R., Higgins, J.A., 2015. Mg and Ca isotope signatures of authigenic dolomite in siliceous deep-sea sediments. Earth and Planetary Science Letters 419, 32–42. doi:10.1016/j.epsl.2015.03.006

Bonifacie, M., Ferry, J.M., Horita, J., Vasconcelos, C., Passey, B.H., Eiler, J.M., 2011. Calibration and applications of the dolomite clumped isotope thermometer to high temperatures. Mineralogical Magazine 75, 551.

Bonifacie, M., Calmels, D., Eiler, J. M., Horita, J., Chaduteau, C., Vasconcelos, C., et al. 2017. Calibration of the dolomite clumped isotope thermometer from 25 to 350°C, and implications for a universal calibration for all (Ca, Mg, Fe)CO_3 carbonates. Geochimica Et Cosmochimica Acta 200, 255–279. doi:10.1016/j.gca.2016.11.028

Brady, J.B., Cherniak, D.J., 2010. Diffusion in Minerals: An Overview of Published Experimental Diffusion Data. Reviews in Mineralogy and Geochemistry 72, 899–920. doi:10.2138/rmg.2010.72.20

Brand, W.A., Assonov, S.S., Coplen, T.B., 2010. Correction for the 17O interference in δ(13C) measurements when analyzing CO2 with stable isotope mass spectrometry (IUPAC Technical Report). Pure and Applied Chemistry 82. doi:10.1351/PAC-REP-09-01-05

Brenner, D. C., Passey, B. H., & Stolper, D. A. (2018). Influence of water on clumped-isotope bond reordering kinetics in calcite. Geochimica Et Cosmochimica Acta 224, 42–63. doi:10.1016/j.gca.2017.12.026

Chai, L., Navrotsky, A., 1996. Synthesis, characterization, and energetics of solid solution along the dolomite-ankerite join, and implications for the stability of ordered CaFe (CO3) 2. American Mineralogist 81, 1141–1147.

Daëron, M., Blamart, D., Peral, M., Affek, H.P., 2016. Absolute isotopic abundance ratios and the accuracy of Δ47 measurements. Chemical Geology 442, 83–96. doi:10.1016/j.chemgeo.2016.08.014

del Real, P. G. A., Maher, K., Kluge, T., Bird, D. K., Brown, G. E., Jr, & John, C. M. (2016). Clumped-isotope thermometry of magnesium carbonates in ultramafic rocks. Geochimica Et Cosmochimica Acta 193, 222–250. doi: 10.1016/j.gca.2016.08.003

Dennis, K.J., Affek, H.P., Passey, B.H., Schrag, D.P., Eiler, J.M., 2011. Defining an absolute reference frame for "clumped" isotope studies of CO2. Geochimica et Cosmochimica Acta 75, 7117–7131. doi:10.1016/j.gca.2011.09.025

Dennis, K.J., Schrag, D.P., 2010. Clumped isotope thermometry of carbonatites as an indicator of diagenetic alteration. Geochimica et Cosmochimica Acta 74, 4110–4122. doi:10.1016/j.gca.2010.04.005

Eiler, J.M., 2011. Paleoclimate reconstruction using carbonate clumped isotope thermometry. Quaternary Science Reviews 30, 3575–3588. doi:10.1016/j.quascirev.2011.09.001

Eiler, J.M., 2007. "Clumped-isotope" geochemistry—The study of naturally-occurring, multiply-substituted isotopologues. Earth and Planetary Science Letters 262, 309–327. doi:10.1016/j.epsl.2007.08.020

Eiler, J.M., Schauble, E., 2004. 18O13C16O in Earth's atmosphere. Geochimica et Cosmochimica Acta 68, 4767–4777.

Farver, J.R., 2010. Oxygen and Hydrogen Diffusion in Minerals. Reviews in Mineralogy and Geochemistry 72, 447–507. doi:10.2138/rmg.2010.72.10

Ferry, J.M., Passey, B.H., Vasconcelos, C., Eiler, J.M., 2011. Formation of dolomite at 40-80 C in the Latemar carbonate buildup, Dolomites, Italy, from clumped isotope thermometry. Geology 39, 571–574. doi:10.1130/G31845.1

Fortier, S.M., Giletti, B.J., 1989. An empirical model for predicting diffusion coefficients in silicate minerals. Science 245, 1481–1484.

Ghosh, P., Adkins, J., Affek, H., Balta, B., Guo, W., Schauble, E.A., Schrag, D., Eiler, J.M., 2006. 13C–18O bonds in carbonate minerals: A new kind of paleothermometer. Geochimica et Cosmochimica Acta 70, 1439–1456. doi:10.1016/j.gca.2005.11.014

Goldsmith, J.R., Heard, H.C., 1961. Subsolidus phase relations in the system $CaCO_3$–$MgCO_3$. The Journal of Geology 45–74.

Graf, D.L., Goldsmith, J.R., 1955. Dolomite—magnesian calcite relations at elevated temperatures and CO 2 pressures. Geochimica et Cosmochimica Acta 7, 109–128.

Gregg, J.M., Bish, D.L., Kaczmarek, S.E., Machel, H.G., 2015. Mineralogy, nucleation and growth of dolomite in the laboratory and sedimentary environment: A review. Sedimentology 62, 1749–1769. doi:10.1111/sed.12202

Henkes, G. A., Passey, B. H., Wanamaker, A. D., Jr., Grossman, E. L., Ambrose, W. G., Jr., & Carroll, M. L. (2013). Carbonate clumped isotope compositions of modern marine mollusk and brachiopod shells. Geochimica et Cosmochimica Acta 106, 307–325. http://doi.org/10.1016/j.gca.2012.12.020

Henkes, G.A., Passey, B.H., Grossman, E.L., Shenton, B.J., Pérez-Huerta, A., Yancey, T.E., 2014. Temperature limits for preservation of primary calcite clumped isotope paleotemperatures. Geochimica et Cosmochimica Acta 139, 362–382. doi:10.1016/j.gca.2014.04.040

Héberger, K., Kemény, S., 1987. On the errors of Arrhenius parameters and estimated rate constant values. Int. J. Chem. Kinet. 19, 171–181.

Jonas, L., Müller, T., Dohmen, R., Baumgartner, L., Putlitz, B., 2015. Transport-controlled hydrothermal replacement of calcite by Mg-carbonates. Geology 43, 779–782.

Jones, B., Luth, R.W., MacNeil, A.J., 2001. Powder X-ray diffraction analysis of homogeneous and heterogeneous sedimentary dolostones. Journal of Sedimentary Research 71, 790–799.

Kolodny, Y., Kaplan, I.R., 1970. Carbon and oxygen isotopes in apatite CO2 and co-existing calcite from sedimentary phosphorite. Journal of Sedimentary Research 40, 954–959.

Lloyd, M.K., Eiler, J.M., Nabelek, P.I., 2017. Clumped isotope thermometry of calcite and dolomite in a contact metamorphic environment. Geochimica et Cosmochimica Acta 197, 323–344. doi:10.1016/j.gca.2016.10.037

Lugli, S., Torres-Ruiz, J., Garuti, G., Olmedo, F., 2000. Petrography and geochemistry of the Eugui magnesite deposit (Western Pyrenees, Spain): evidence for the development of a peculiar zebra banding by dolomite replacement. Economic Geology 95, 1775–1791.

Machel, H.G., 2004. Concepts and models of dolomitization: a critical reappraisal. Geological Society, London, Special Publications 235, 7. doi:10.1144/GSL.SP.2004.235.01.02

Martinez, I., Zhang, J., Reeder, R.J., 1996. In situ X-ray diffraction of aragonite and dolomite at high pressure and high temperature: Evidence for dolomite breakdown to aragonite and magnesite. American Mineralogist 81, 611–624.

Murray, S.T., Arienzo, M.M., Swart, P.K., 2016. Determining the. Geochimica et Cosmochimica Acta 174, 42–53. doi:10.1016/j.gca.2015.10.029

Murray, S.T., Swart, P.K., 2017. Evaluating formation fluid models and calibrations using clumped isotope paleothermometry on Bahamian dolomites. Geochimica et Cosmochimica Acta 206, 73–93. doi:10.1016/j.gca.2017.02.021

Nagy, T., Turányi, T., 2011. Uncertainty of Arrhenius parameters. Int. J. Chem. Kinet. 43, 359–378. doi:10.1002/kin.20551

Navrotsky, A., Capobianco, C., 1987. Enthalpies of formation of dolomite and of magnesian calcites. American Mineralogist 72, 782–787.

O'Neil, J.R., Epstein, S., 1966. Oxygen Isotope Fractionation in the System Dolomite-Calcite-Carbon Dioxide. Science 152, 198–201.

Passey, B.H., Henkes, G.A., 2012. Carbonate clumped isotope bond reordering and geospeedometry. Earth and Planetary Science Letters 351–352, 223–236. doi:10.1016/j.epsl.2012.07.021

Passey, B.H., Levin, N.E., Cerling, T.E., Brown, F.H., Eiler, J.M., 2010. High-temperature environments of human evolution in East Africa based on bond ordering in paleosol carbonates. Proceedings of the National Academy of Sciences 107, 11245–11249. doi:10.1073/pnas.1001824107

Reeder, R.J., Markgraf, S.A., 1986. High-temperature crystal chemistry of dolomite. American Mineralogist 71, 795–804.

Reeder, R.J., Nakajima, Y., 1982. The nature of ordering and ordering defects in dolomite. Phys Chem Minerals 8, 29–35.

Reeder, R.J., Wenk, H.R., 1983. Structure refinements of some thermally disordered dolomites. American Mineralogist 68, 769–776.

Rosenbaum, J., Sheppard, S.M.F., 1986. An isotopic study of siderites, dolomites and ankerites at high temperatures. Geochimica et Cosmochimica Acta 50, 1147–1150.

Ryb, U., Lloyd, M.K., Stolper, D.A., Eiler, J.M., 2017. The clumped-isotope geochemistry of exhumed marbles from Naxos, Greece. Earth and Planetary Science Letters 470, 1–12. doi:10.1016/j.epsl.2017.04.026

Schauble, E.A., Ghosh, P., Eiler, J.M., 2006. Preferential formation of 13C–18O bonds in carbonate minerals, estimated using first-principles lattice dynamics. Geochimica et Cosmochimica Acta 70, 2510–2529. doi:10.1016/j.gca.2006.02.011

Schauer, A.J., Kelson, J., Saenger, C., Huntington, K.W., 2016. Choice of 17O correction affects clumped isotope (Δ47) values of CO2 measured with mass spectrometry. Rapid Commun. Mass Spectrom. 30, 2607–2616. doi:10.1002/rcm.7743

Shenton, B.J., Grossman, E.L., Passey, B.H., Henkes, G.A., Becker, T.P., Laya, J.C., Pérez-Huerta, A., Becker, S.P., Lawson, M., 2015. Clumped isotope thermometry in deeply buried sedimentary carbonates: The effects of bond reordering and recrystallization. Geological Society of America Bulletin. doi:10.1130/B31169.1

Sheppard, S.M.F., Schwarcz, H.P., 1970. Fractionation of carbon and oxygen isotopes and magnesium between coexisting metamorphic calcite and dolomite. Contrib Mineral Petrol 26, 161–198. doi:10.1007/BF00373200

Shirasaka, M., Takahashi, E., Nishihara, Y., 2002. In situ X-ray observation of the reaction dolomite= aragonite+ magnesite at 900–1300 K. American Mineralogist 87, 922–930.

Stolper, D.A., Eiler, J.M., 2015. The kinetics of solid-state isotope-exchange reactions for clumped isotopes: A study of inorganic calcites and apatites from natural and experimental samples. American Journal of Science 315, 363–411. doi:10.2475/05.2015.01

Urosevic, M., Rodriguez-Navarro, C., Putnis, C.V., Cardell, C., Putnis, A., Ruiz-Agudo, E., 2012. In situ nanoscale observations of the dissolution of. Geochimica et Cosmochimica Acta 80, 1–13. doi:10.1016/j.gca.2011.11.036

Wang, Z., Schauble, E.A., Eiler, J.M., 2004. Equilibrium thermodynamics of multiply substituted isotopologues of molecular gases. Geochimica et Cosmochimica Acta 68, 4779–4797. doi:10.1016/j.gca.2004.05.039

Warren, J., 2000. Dolomite: occurrence, evolution and economically important associations. Earth-Science Reviews 52, 1–81.

Winkelstern, I.Z., Lohmann, K.C., 2016. Shallow burial alteration of dolomite and limestone clumped isotope geochemistry. Geology 44, 467–470. doi:10.1130/G37809.1

Yelon, A., Movaghar, B., Branz, H.M., 1992. Origin and Consequences of the Compensation (Meyer-Neldel) Law. Physical Review B 46, 12244–12250.

Zhang, Y., 2010. Diffusion in Minerals and Melts: Theoretical Background. Reviews in Mineralogy and Geochemistry 72, 5–59. doi:10.2138/rmg.2010.72.2

Zhang, Y., Stolper, E.M., Ihinger, P.D., 1995. Kinetics of the reaction H2O+ O= 2OH in rhyolitic and albitic glasses: preliminary results. American Mineralogist 80, 593–612.

Zheng, Y.F., Fu, B., 1998. Estimation of oxygen diffusivity from anion porosity in minerals. Geochem. J. 32, 71–89.

Table 1:

Heating T (°C)	Heating time (hrs)	P_{CO2} (MPa)	n	$\delta^{13}C$ (VPDB) (‰)	$\delta^{13}C$ 1σ s.d.	$\delta^{18}O$ (VPDB) (‰)	$\delta^{18}O$ 1σ s.d.	Δ_{47} (ARF) (‰)	Δ_{47} 1σ s.e.
N/A	**0**	**N/A**	35	2.60	0.22	-14.61	1.02	0.452	0.002
409	**42**	70.0	4	2.37	0.02	-14.63	0.09	0.433	0.004
	311	67.9	5	2.26	0.07	-15.05	1.42	0.395	0.021
460	**86**	50.5	5	2.50	0.06	-13.85	0.30	0.376	0.010
	314	72.0	7	2.59	0.28	-14.19	0.70	0.390	0.007
486	**2.4**	67.1	3	2.51	0.10	-13.70	0.52	0.412	0.012
	24	69.4	7	2.71	0.04	-13.89	0.14	0.401	0.006
	68.8	53.0	4	2.68	0.04	-14.01	0.09	0.349	0.018
	169.4	43.5	3	2.80	0.04	-13.98	0.09	0.348	0.004
	238.2	57.4	3	2.49	0.05	-14.14	0.10	0.335	0.006
	455.28	66.3	5	2.41	0.04	-14.08	0.12	0.333	0.008
511	**1**	62.8	3	2.27	0.01	-14.90	0.05	0.401	0.005
	2.5	63.2	5	2.40	0.04	-14.27	0.11	0.411	0.003
	12.83	63.1	4	2.14	0.03	-14.53	0.08	0.348	0.008
	48.2	53.4	3	2.39	0.03	-14.92	0.10	0.342	0.007
	65	61.4	4	2.49	0.10	-14.39	0.28	0.346	0.009
	160	61.9	4	1.97	0.16	-14.40	0.69	0.326	0.012
563	**1**	70.6	4	2.70	0.12	-14.19	0.11	0.359	0.008
	17	61.2	5	2.17	0.28	-14.35	0.06	0.318	0.008
	67.75	71.0	5	2.55	0.03	-14.48	0.11	0.311	0.011
	160.5	69.6	3	2.66	0.19	-14.35	0.57	0.300	0.026
614	**0.08**	59.0	4	2.14	0.02	-14.87	0.03	0.396	0.005
	0.13	69.4	3	2.64	0.04	-14.19	0.06	0.388	0.003
	0.25	71.0	3	2.09	0.03	-14.25	0.08	0.344	0.012
	0.42	78.4	4	1.99	0.12	-14.70	0.36	0.331	0.004
	1	55.8	3	2.84	0.03	-14.40	0.10	0.326	0.007
	3	73.0	3	2.32	0.01	-14.88	0.06	0.311	0.003
	4.07*	70.3	7	1.85	0.10	-15.13	0.31	0.338	0.005
	64	74.6	7	2.07	0.13	-14.79	0.25	0.323	0.010
717	**0.08**	64.2	1	2.48	0.15	-14.24	0.15	0.302	0.017
	0.75	60.5	3	2.53	0.03	-14.54	0.07	0.290	0.007
	15.25	55.8	4	2.24	0.14	-14.66	0.37	0.322	0.010

Table 1: Mean $\delta^{13}C$, $\delta^{18}O$, and Δ_{47} values of dolomite from all heating experiments and the unheated starting material. Reported uncertainties on $\delta^{13}C$ and $\delta^{18}O$ are 1σ standard deviations of individual measurements. Uncertainties on Δ_{47} values are 1σ standard errors. ^{18}O compositions of dolomite fragments are calculated from $\delta^{18}O$ values of CO_2 using a 90 °C dolomite–CO_2 common acid bath fractionation of: $^{18}\alpha$ = 1.009218 (see Section 2.3). Δ_{47} are reported in the CO_2-equilibrated absolute reference frame, and corrected to the 25 °C acid scale by adding a fractionation factor of 0.092 ‰. Asterix denotes an experiment where aberrant $\delta^{13}C$, $\delta^{18}O$, and Δ_{47}

values all suggest minor contamination by a secondary carbonate, so this sample is omitted from analyses and model fits.

Table 2:

T--Δ47 calibration		$\ln(K_c)$	E_c	$\ln(K_d)$	E_d	$\ln(K_2)$	E_2
Bonifacie	Best fit to measured data	20.2	213.8	15.3	161.2	5.8	96.9
	Mean of acceptable fits	20.6	217.2	15.1	160.3	6.3	100.6
	1σ standard deviation	5.2	32.8	3.3	23.5	5.0	33.4
Schauble + Bonifacie	Best fit to measured data	16.6	193.7	16.1	166.7	8.3	113.1
	Mean of acceptable fits	14.2	179.5	15.7	164.3	8.2	112.6
	1σ standard deviation	6.6	40.5	3.5	25.4	4.4	32.1
Lloyd	Best fit to measured data	18.8	205.6	15.5	162.5	6.8	103.2
	Mean of acceptable fits	18.5	204.3	15.2	160.6	6.9	103.9
	1σ standard deviation	4.8	30.2	3.3	21.2	4.6	32.0

Table 2: Dolomite Δ_{47} reordering parameters for the Henkes et al. (2014) transient defect/equilibrium defect model. 'Best fit' parameters were generated using an error-weighted least squares global fit to the mean measured data reported in Table 1. Mean and 1σ s.d. of acceptable fits are the averages and standard deviations for each parameter based on fits to ~10,000 Monte Carlo simulations of the underlying Δ_{47} values. Activation energies are all reported in kJ/mol. Pre-exponential factors are reported in s^{-1}.

Table 3:

T--Δ47 calibration		$\ln(K0_f)$	Ea_f	$\ln(K0_{diff,single})$	$Ea_{diff,single}$	m_p
Bonifacie	Best fit to measured data	21.5	194.5	31.8	273.6	0.0668
	Mean of acceptable fits	21.2	192.8	32.3	276.5	0.0663
	1σ standard deviation	1.2	7.6	1.8	11.9	0.0063
Schauble + Bonifacie	Best fit to measured data	25.3	220.1	31.5	275.3	0.0766
	Mean of acceptable fits*	24.2	214.0	31.9	278.8	0.0720
	1σ standard deviation	2.1	13.5	2.5	16.3	0.015
Lloyd	Best fit to measured data	22.6	201.7	33.1	283.0	0.0734
	Mean of acceptable fits	24.3	212.7	32.3	278.6	0.0685
	1σ standard	2.7	16.8	2.4	15.9	0.0132

deviation

Table 3: Dolomite Δ_{47} reordering parameters for the Stolper and Eiler (2015) exchange–diffusion model. Sources of fits, and units, are summarized in Table 2. Asterix denotes the recommended parameter set for forward modeling dolomite Δ_{47}reordering.

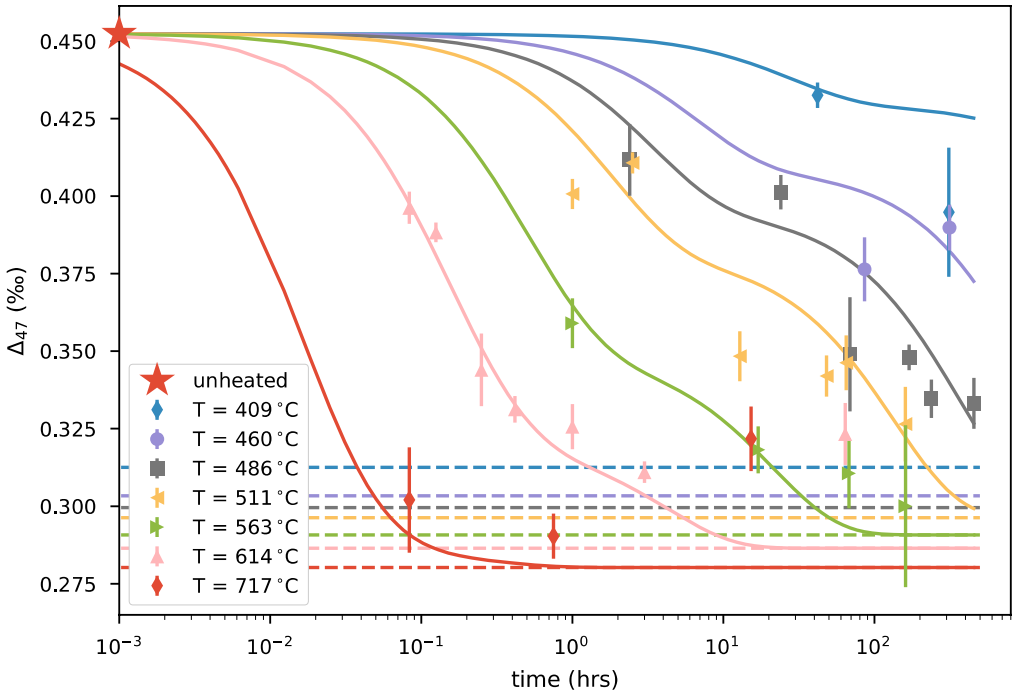

Figure 1: Error-weighted global least squares fit to dolomite heating experiments using the transient defect/equilibrium defect model of Henkes et al. (2014) (Eqn. 10). Red star is the mean unheated initial composition. Other symbols are mean of replicate measurements of heating experiments, with 1σ standard errors. Solid lines are the global fit to the data. The 717 °C trend apparently begins below the initial composition because significant reordering occurs in the first 10^{-3} hours (not shown on this scale). Dashed lines are equilibrium Δ_{47} values for every temperature according to the Schauble + Bonifacie calibration.

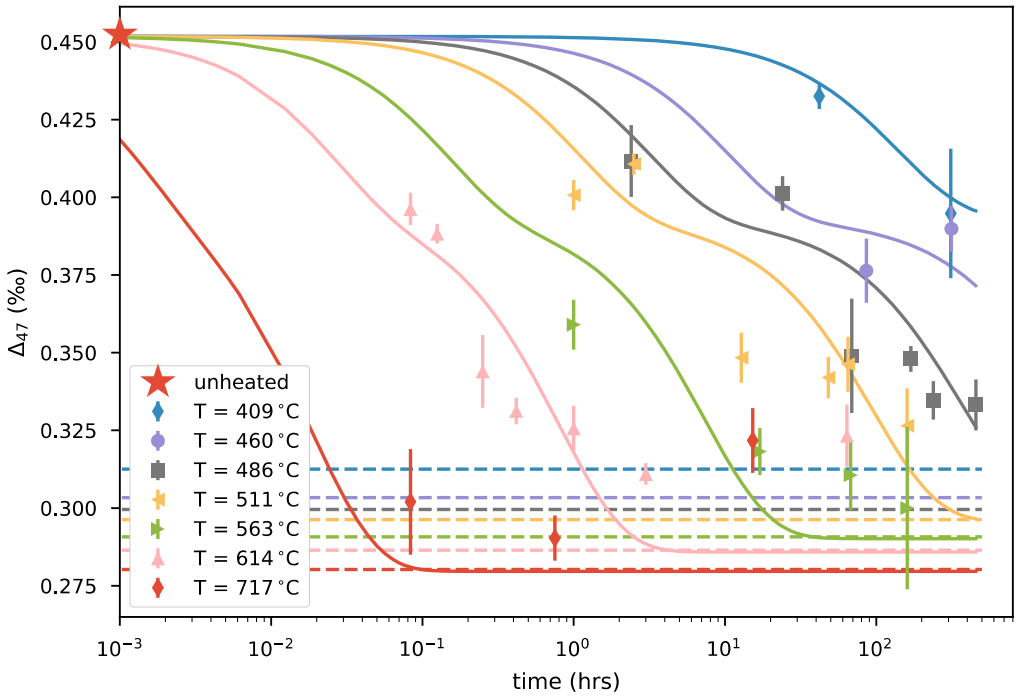

Figure 2: Error-weighted global least squares fit to dolomite heating experiments using the exchange-diffusion model of Stolper and Eiler (2015) (Eqns. 12–14). Red star is the mean unheated initial composition. Other symbols are mean of replicate measurements of heating experiments, with 1σ standard errors. Solid lines are the global fit to the data. The 717 °C trend apparently begins below the initial composition because significant reordering occurs in the first 10^{-3} hours (not shown on this scale). Dashed lines are equilibrium Δ_{47} values for every temperature, according to the Schauble + Bonifacie calibration.

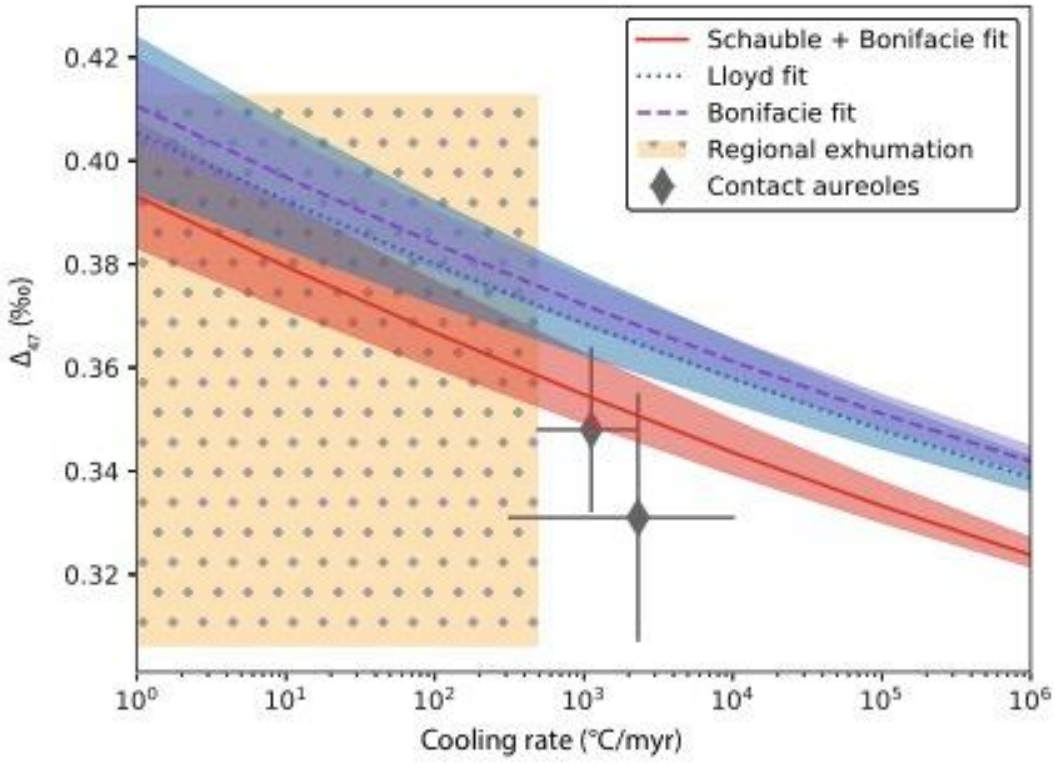

Figure 3: Predicted dependence of dolomite Δ_{47} apparent equilibrium blocking temperature on cooling rate, and the measured apparent equilibrium blocking temperatures of natural dolomite marbles. Shaded regions denote 2σ uncertainties on predictions of the exchange-diffusion model for three different Δ_{47}–T calibrations. Cooling rates with uncertainties for the Notch Peak and Predazzo contact aureoles were estimated from conductive cooling models described in Lloyd et al. (2017). Low temperature cooling rates from regionally exhumed terranes are rarely known with useful precision, and the range of apparent equilibrium temperatures measured in such systems is larger than would be expected if regional exhumation was the sole determining variable (c.f., Ryb et al. 2017). Thus, we plot only the rough region over which these processes are likely to operate.

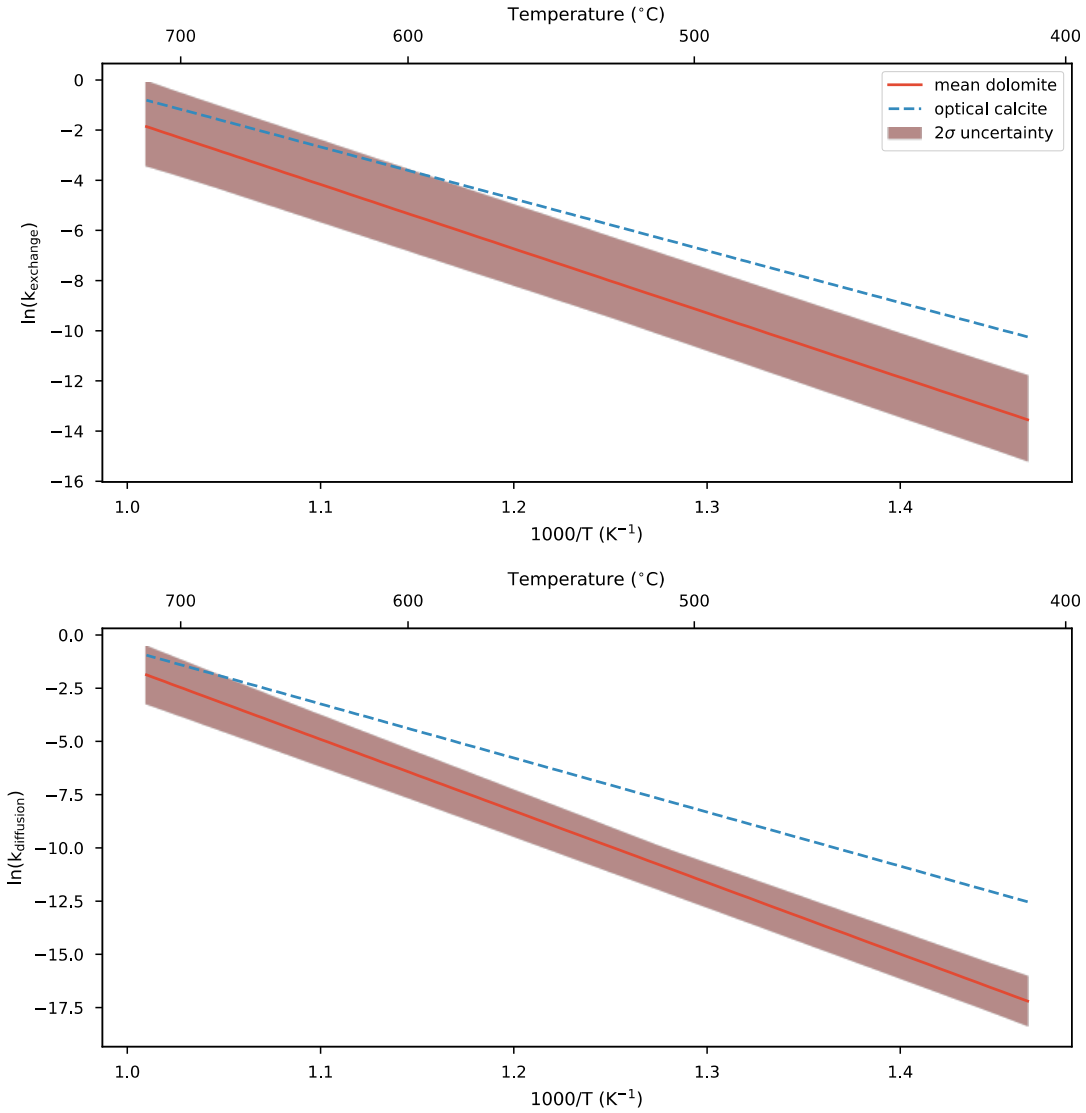

Figure 4: Arrhenius plots for the rate constants for the exchange and diffusion components of the Stolper and Eiler (2015) model (Schauble + Bonifacie calibration). Dolomite rate constants (and uncertainties) from this study are compared with optical calcite rate constants from this previous publication.

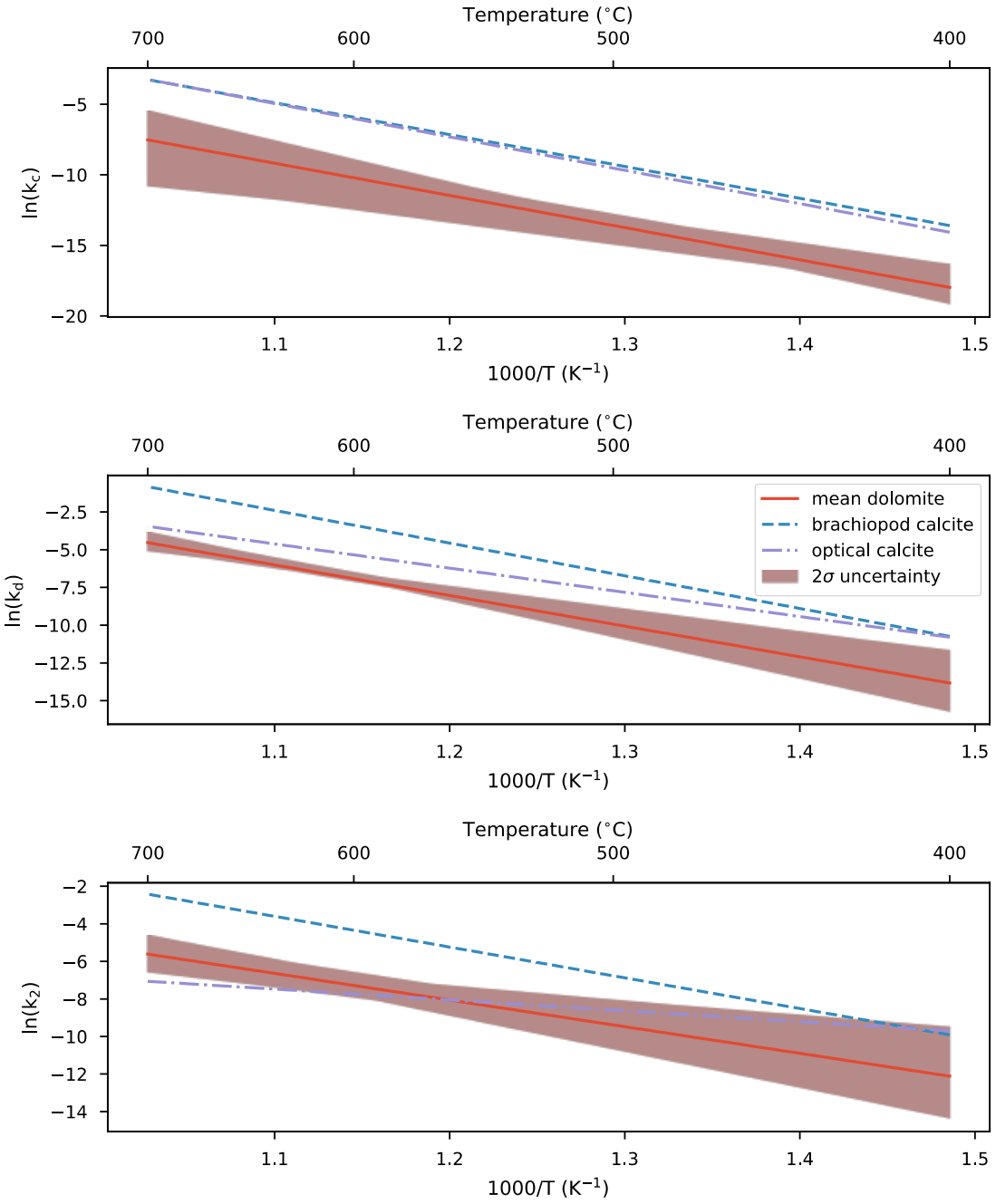

Figure 5: Arrhenius plots for the rate constants for the equilibrium component, transient component, and annealing rate on the transient component, for the Δ_{47} reordering model of Henkes et al. (2014) (Schauble + Bonifacie calibration). These are compared to the parameters for optical calcite and brachiopod calcite reported therein.

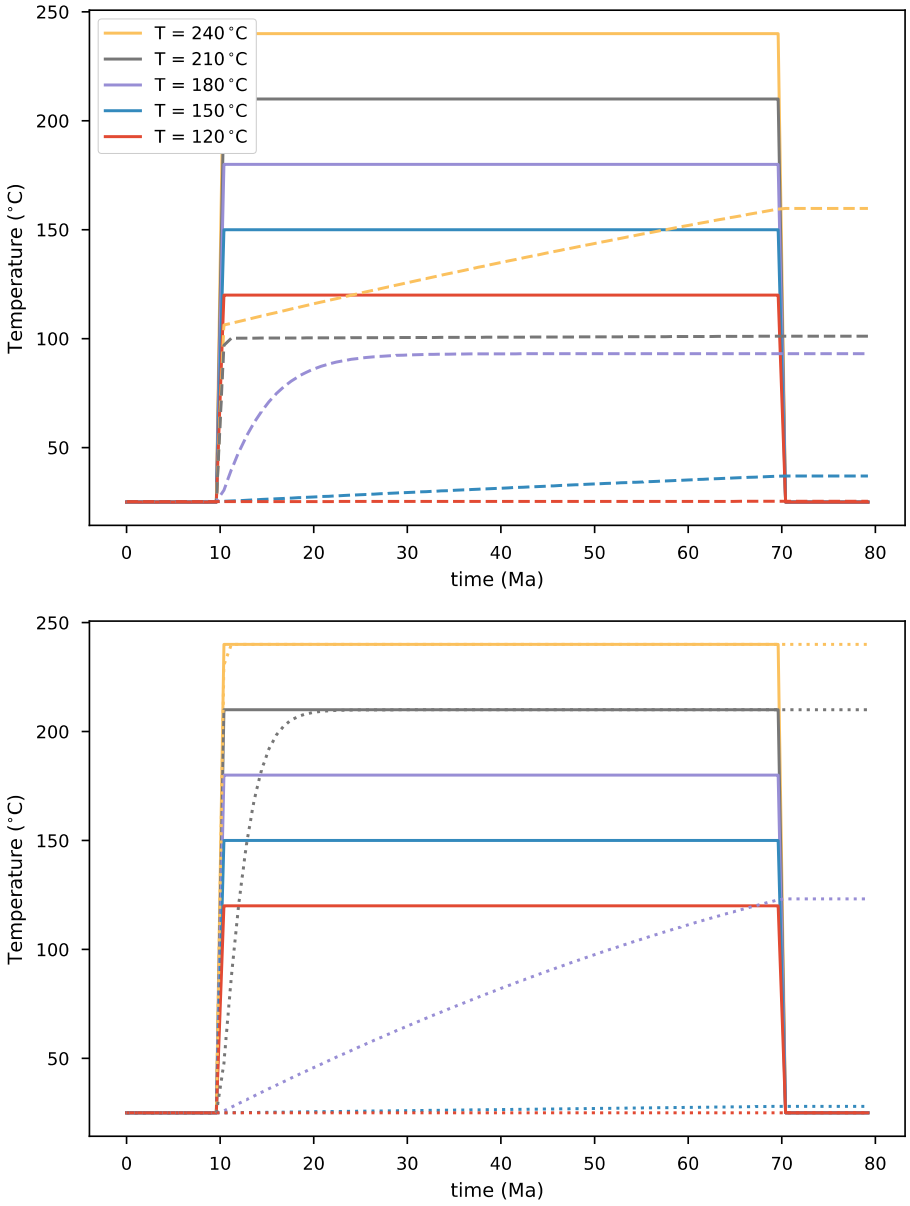

Figure 6: Instantaneous isothermal heating models of dolomite Δ_{47} reordering. Solid lines denote the true temperature-time path of each run. Dashed lines (top panel) are dolomite Δ_{47} apparent equilibrium temperatures predicted using the exchange-diffusion model for each T-t path. Dotted lines (bottom panel) are the dolomite Δ_{47} temperatures predicted using the transient defect/equilibrium defect model. Uncertainties on kinetic parameters are omitted here for clarity.

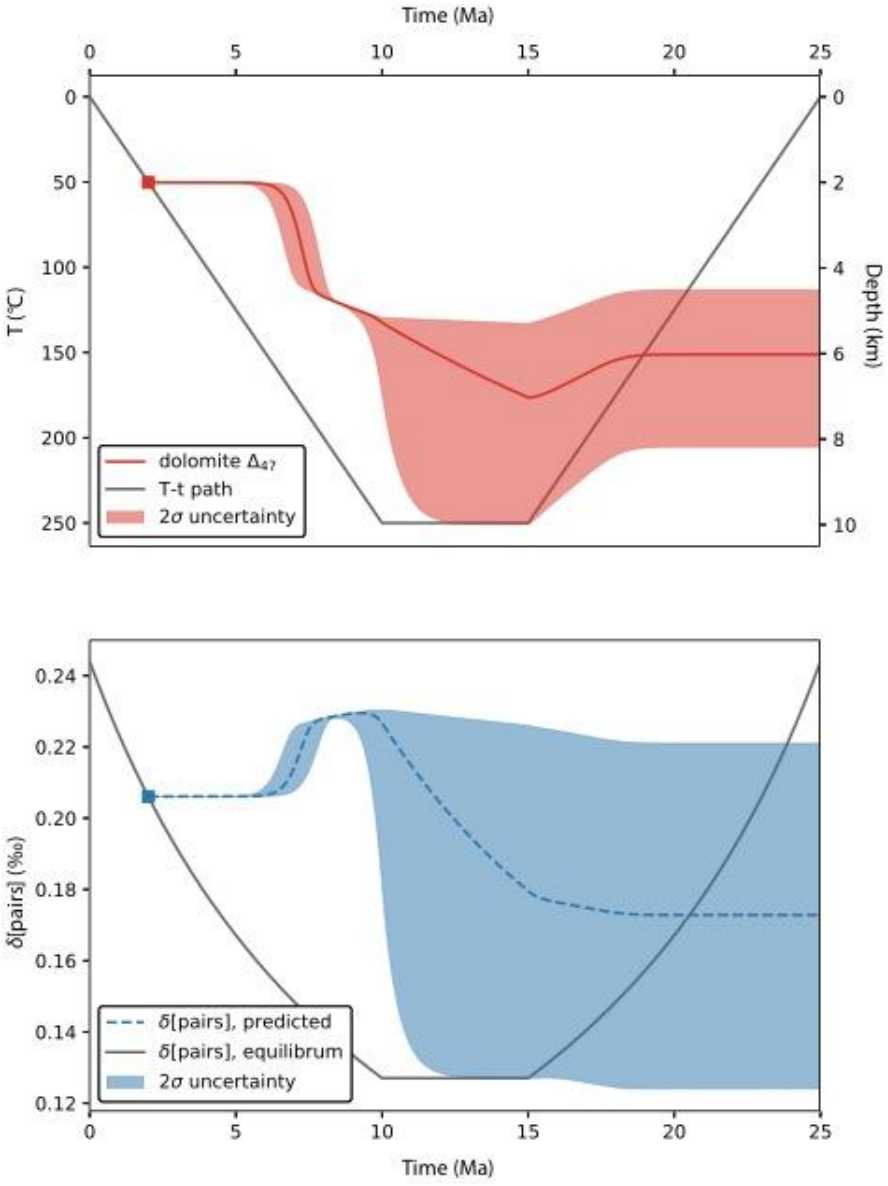

Figure 7: Expected reordering behavior and corresponding pair concentrations of the dolomite Δ_{47} thermometer using the exchange-diffusion model in a simple burial-exhumation scenario. Shaded areas denote 2σ confidence limits for the respective property. Predicted and equilibrium pair concentrations are represented in delta notation relative to the stochastic (random) pair concentration for this sample's bulk composition: $\delta[\text{pair}] = ([\text{pair}]_{\text{predicted or equilibrated}} / [\text{pair}]_{\text{rand}} - 1)$ (in ‰). This model assumes no recrystallization after initial dolomite and calcite formation. A flexible software package for performing similar forward Δ_{47} reordering models

for any user-specified T-t path is freely available and updated regularly (www.github.com/maxmansaxman/Clumpy_reordering_model_distribution).